

# Reservoir-engineered spin squeezing: macroscopic even-odd effects and hybrid-systems implementations

Peter Groszkowski<sup>1</sup>, Martin Koppenhöfer<sup>1</sup>, Hoi-Kwan Lau<sup>2</sup>, A. A. Clerk<sup>1</sup>

<sup>1</sup>*Pritzker School of Molecular Engineering, University of Chicago, Chicago, IL, USA*

<sup>2</sup>*Department of Physics, Simon Fraser University, Burnaby, BC, Canada*

(Dated: April 22, 2021)

We revisit the dissipative approach to producing and stabilizing spin-squeezed states of an ensemble of  $N$  two-level systems, providing a detailed analysis of two surprising yet generic features of such protocols. The first is a macroscopic sensitivity of the steady state to whether  $N$  is even or odd. We discuss how this effect can be avoided (if the goal is parity-insensitive squeezing), or could be exploited as a new kind of sensing modality with single-spin sensitivity. The second effect is an anomalous emergent long timescale and a “prethermalized” regime that occurs for even weak single-spin dephasing. We also discuss a general hybrid-systems approach for implementing dissipative spin squeezing that does not require squeezed input light or complex multi-level atoms, but instead makes use of bosonic reservoir-engineering ideas. Our protocol is compatible with a variety of platforms, including trapped ions, NV defect spins coupled to diamond optomechanical crystals, and spin ensembles coupled to superconducting microwave circuits.

## I. INTRODUCTION

Among the most sought after states in quantum metrology are spin-squeezed states, highly entangled states of spin-1/2 ensembles that enable parameter sensing with a sensitivity better than the standard quantum limit, even reaching fundamental Heisenberg-limit scaling [1, 2]. The standard approach for producing these states is to unitarily evolve an initial product state under a collective spin-spin interaction Hamiltonian. While many interactions are possible, the most widely studied one is the one-axis twist (OAT) Hamiltonian [1], which has been realized in a number of ground-breaking experiments [3–6]. It unfortunately is not capable of achieving Heisenberg-limited squeezing even in the ideal case [2]. An alternate, more complex interaction Hamiltonian is the two-axis twist (TAT) Hamiltonian [1, 7–10], which, while more resource intensive, allows achieving Heisenberg-limited scaling.

While easy to understand, tailored unitary-evolution is not the only approach to spin squeezing. An alternative is to use the general strategy of reservoir engineering [11], where tailored dissipation is exploited to both produce and *stabilize* a non-trivial state of interest, *i.e.*, a spin-squeezed state (see Fig. 1). The dissipative approach in principle has several advantages: the spin-squeezed state is stabilized in the steady state (as opposed to just prepared at a specific instant of time), the stabilization is largely insensitive to the initial state of the ensemble, and one can achieve Heisenberg-limited scaling. The dissipative stabilization of bosonic squeezed states has been studied extensively both theoretically [12–14] and experimentally [15–20]. Corresponding schemes for spin squeezing have also been studied theoretically. The earliest works analyzed

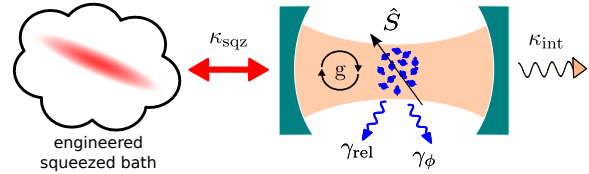


FIG. 1. Schematic representation of a generic approach to generate dissipative spin squeezing by coupling spins to a bosonic mode that interacts with a squeezed reservoir. The squeezing rate experienced by the cavity is governed by the parameter  $\kappa_{\text{sqz}}$ , while  $g$  represents the spin-cavity coupling strength. Limiting factors to the protocol’s performance are the intrinsic photon-loss rate  $\kappa_{\text{int}}$ , the local spin-relaxation rate  $\gamma_{\text{rel}}$ , and the local spin-dephasing rate  $\gamma_{\phi}$ .

schemes where atoms are directly illuminated with squeezed light. Both the cases of two-level atoms [21–23] and V-type multilevel atoms [24] were studied. More recently, it was shown theoretically that the same effective dissipative dynamics could be realized by using Raman processes in driven multilevel atoms coupled to a lossy cavity [9, 25].

In this work, we revisit the dissipative approach to spin squeezing. Our work complements previous studies both by discussing a powerful, alternative method for implementing these schemes, as well as describing surprising phenomena that had not been fully analyzed in the past. In terms of implementation, we analyze a very general hybrid-systems approach that harnesses bosonic dissipative squeezing. We consider a spin-ensemble which is resonantly coupled to a cavity mode (via a standard Tavis-Cummings [26] interaction), which is in turn coupled to an effective squeezed reservoir (see Fig. 1). While this latter reservoir could be realized using

squeezed input light, there are also simpler methods. In particular, it can be implemented using only *classical* optical or microwaves drives by harnessing existing dissipative bosonic squeezing schemes. Such schemes produce an effective squeezed dissipator for the cavity, and have been experimentally implemented in wide variety of platforms, including optomechanics [15], trapped ions [16] and superconducting circuits [20]. We demonstrate that this hybrid-systems approach to dissipative spin squeezing can reach the Heisenberg limit, and also outperform OAT in the presence of single-spin  $T_1$  decay. Note that unlike the Raman scheme of Ref. 25, which requires atoms with a specific 4-level configuration, the approach here only requires standard two-level atoms, making it compatible with a wide variety of systems (including possibly solid-state systems such as ensembles of NV defect spins in diamond [27]).

Our work also analyzes surprising phenomena that were not fully discussed previously. Perhaps most striking is the extreme sensitivity of dissipative spin squeezing to the parity of the total number of spins  $N$ : the steady state is macroscopically different for  $N$  spins versus  $N + 1$  spins. While this effect was implicitly contained in the results of Agarwal and Puri [21, 22], we provide here a fully qualitative and quantitative analysis. We discuss how this effect can be avoided (if one wants strong spin squeezing independent of parity), and how it could also be exploited as a new kind of sensing modality. We also make a surprising connection to a non-dissipative many-body system, the antiferromagnetic Lipkin-Meshkov-Glick (LMG) model [28, 29].

A second surprising and new phenomenon we describe is the interplay between collective dissipative spin squeezing dynamics and noncollective single-spin dephasing. As we show, this results in an extremely long relaxation timescale in the system (*i.e.*, inverse dissipative gap) which grows with system size  $N$ . At a fundamental level, the effect has parallels to prethermalization behavior observed in weakly nonintegrable systems (see, *e.g.*, [30, 31]). At a practical level, we show that even infinitesimally weak single-spin dephasing dramatically impairs the steady-state spin squeezing to at most  $-3$  dB. We also show that this need not be a limitation: large amounts of squeezing are possible in the prethermalized regime, or by deliberately adding very small levels of single-spin relaxation.

The remainder of this paper is organized as follows: In Sec. II, we outline the key idea behind the standard approach to dissipative spin squeezing as well as summarize our generic protocol. In Sec. III, we explore the even-odd effect and briefly discuss connections to sensing. In Sec. IV, we carefully analyze the performance of our dissipative spin

squeezing protocol in the presence of single-spin dissipation, showing that the steady-state squeezing it generates can outperform the transient squeezing produced by standard OAT. In Sec. V, we discuss the emergence of anomalously slow relaxation times, while in Sec. VI, we discuss in more detail how our protocol could be implemented in a variety of different physical systems. Conclusions and a summary are presented in Sec. VII.

## II. MODEL AND THE BASIC DISSIPATIVE SQUEEZING PROTOCOL

The reservoir engineering approach to spin squeezing requires one to construct a nontrivial dissipative environment for the spins. In this section, we review the idealized spin-only quantum master equation that describes the needed dissipative dynamics [21, 22]. We then present a more realistic model that corresponds to the generic, experimentally-friendly hybrid-systems setup sketched in Fig. 1, where a spin ensemble is coupled to a cavity (or other bosonic mode), which is in turn coupled to an engineered squeezed reservoir.

Throughout this paper, we quantify the amount of metrologically-useful spin squeezing (*i.e.*, as relevant to a standard Ramsey measurement) using the Wineland parameter [2, 32]. It is defined as

$$\xi_R^2 \equiv N \frac{\langle \Delta \hat{S}_\perp^2 \rangle}{\langle \hat{\mathbf{S}} \rangle^2}, \quad (1)$$

where  $\langle \Delta \hat{S}_\perp^2 \rangle$  is the minimum variance in a direction perpendicular to the direction of the mean of the collective spin and  $\hat{\mathbf{S}} \equiv (\hat{S}_x, \hat{S}_y, \hat{S}_z)$  is the vector of spin operators.

### A. Idealized spin-only model

We consider the following quantum master equation acting on the Hilbert space of  $N$  spin-1/2 particles,

$$\dot{\hat{\rho}} = \Gamma \mathcal{D} \left[ \hat{\Sigma}[r] \right] \hat{\rho}, \quad (2)$$

where we introduced the operator

$$\hat{\Sigma}[r] = \cosh(r) \hat{S}_- - \sinh(r) \hat{S}_+. \quad (3)$$

Here,  $\Gamma$  is the coupling rate to the engineered reservoir,  $r$  characterizes the squeezing strength, and  $\mathcal{D}[\hat{z}] \hat{\rho} = \hat{z} \hat{\rho} \hat{z}^\dagger - \{\hat{z}^\dagger \hat{z}, \hat{\rho}\}/2$  is the standard Lindblad dissipative superoperator. We also introduced the collective spin operators  $\hat{S}_\pm = \hat{S}_x \pm i \hat{S}_y$  with

$\hat{S}_k = \frac{1}{2} \sum_{j=1}^N \hat{\sigma}_k^{(j)}$  for  $k \in \{x, y, z\}$ , where  $\hat{\sigma}_k^{(j)}$  denotes a standard Pauli matrix acting on the  $j$ th spin. Here,  $\hat{\Sigma}[r]$  is analogous to a standard bosonic Bogoliubov annihilation operator, where bosonic raising and lowering operators have been replaced by  $\hat{S}_+$  and  $\hat{S}_-$  respectively. Similar to reservoir-engineered bosonic squeezing [13], the desired squeezed state will correspond to the vacuum of this operator.

To be more explicit, Refs. 21 and 22 showed that, for even  $N$ , Eq. (2) has pure steady states that correspond to zero-eigenvalue eigenstates (*i.e.*, “dark states”) of  $\hat{\Sigma}[r]$ ,

$$\hat{\Sigma}[r] |\psi_{\text{dk}}[j; r]\rangle = 0. \quad (4)$$

Since Eq. (2) conserves the total angular momentum  $j$ , there is a dark state for each allowed value of  $j$ . Each  $|\psi_{\text{dk}}[j; r]\rangle$  has a mean spin polarization in the  $z$  direction, and exhibits squeezing (anti-squeezing) of  $\hat{S}_y$  ( $\hat{S}_x$ ). The choice of the squeezing axis is determined by the relative phase between the  $\hat{S}_+$  and  $\hat{S}_-$  terms in Eq. (3), which is chosen here to be  $-1$ . If the system is initialized in an arbitrary state with a definite value of  $j$ , the dissipative dynamics will relax the system to a dark state in this subspace. For states in the maximum-angular-momentum subspace  $j = j_{\text{max}} = N/2$ , the relaxation timescale (*i.e.*, the inverse dissipative gap of the Liouvillian) is  $\propto 1/NT$ , see Sec. III. Note that the dark states with  $j < j_{\text{max}}$  are not unique, since the corresponding angular-momentum subspaces are degenerate [33]. However, if the initial state and the dynamics are invariant under permutation of spins, the system will only explore permutationally invariant states [34], and there is a unique dark state for each  $j$  subspace, see App. E 1.

As detailed in App. D, the dark states can be expressed in the form [22, 23]

$$|\psi_{\text{dk}}[j; r]\rangle = \mathcal{N}(r) e^{\theta \hat{S}_z} |j, 0\rangle_y, \quad (5)$$

where  $|j, m\rangle_y$  denotes an eigenstate of  $\hat{S}^2$  and  $\hat{S}_y$ ,  $\mathcal{N}(r)$  is a normalization constant, and we defined  $\theta = \ln \sqrt{\tanh(r)}$ . In terms of the eigenstates  $|j, m\rangle$  of  $\hat{S}^2$  and  $\hat{S}_z$ , these states read as follows.

$$|\psi_{\text{dk}}[j; r]\rangle = \sum_{m=-j}^j c_m^{(j)}(r) |j, m\rangle, \quad (6)$$

with the coefficients

$$\begin{aligned} c_{-j+2k}^{(j)}(r) &= \binom{j}{k} \sqrt{\binom{2j}{2k}^{-1}} \tanh^k(r) c_{-j}^{(j)}(r), \\ c_{-j+2k+1}^{(j)}(r) &= 0, \end{aligned} \quad (7)$$

where  $k \in \{0, \dots, j\}$  and  $c_{-j}^{(j)}(r)$  is a normalization constant.

The parameter  $r$  controls the amount of squeezing in the steady state. If we initialize the system in an arbitrary state with  $j = N/2$ , the resulting pure steady state is squeezed, with  $\xi_R^2 \rightarrow 2/(N+2)$  in the large- $r$  limit. This corresponds to Heisenberg-limited spin squeezing, and thus outperforms both the standard quantum limit (*i.e.*,  $\xi_R^2 \propto 1/\sqrt{N}$ ) as well as the maximum squeezing possible with an ideal OAT interaction ( $\xi_R^2 \propto 1/N^{2/3}$ ). Note that a standard leading-order Holstein-Primakoff approximation could be used to map Eq. (2) to a bosonic squeezing dissipator; however, this would not let one understand the ultimate saturation of squeezing (with increasing  $r$ ) to the Heisenberg-limited value.

## B. Hybrid-systems approach to dissipative spin squeezing

As noted in the introduction, previous studies have analyzed methods for realizing the dissipative dynamics in Eq. (2). These methods either required direct driving of spins with squeezed light [22, 24] (which is experimentally challenging), or the use of Raman processes in structured four-level atoms [9, 25] (which is not applicable to generic two-level systems). We present here a method, generic approach that takes a hybrid-systems approach: a cavity (or other bosonic mode) is coupled both to an ensemble of two-level systems, as well as to an engineered, bosonic squeezed reservoir (see Fig. 1). As discussed, such a bosonic squeezed reservoir can be realized using only classical driving fields, and has been implemented in a variety of different experiments [15, 16, 20]. We discuss specific implementation strategies of this general approach in Sec. VI; here, we present the general structure of the overall master equation.

To this end, we consider a spin ensemble that is resonantly coupled (with interaction strength  $g$ ) to a bosonic mode (with lowering operator  $\hat{a}$ ). In the rotating frame, the Hamiltonian is

$$\hat{H} = g(\hat{a}^\dagger \hat{S}_- + \hat{a} \hat{S}_+). \quad (8)$$

We further assume that this mode is coupled both to an engineered squeezed reservoir (with coupling rate  $\kappa_{\text{sqz}}$  and squeezing parameter  $r$ ) as well as subject to unwanted zero-temperature loss (at rate  $\kappa_{\text{int}}$ ). The quantum master equation is then

$$\begin{aligned} \dot{\hat{\rho}} &= -i[\hat{H}, \hat{\rho}] + \kappa_{\text{sqz}} \mathcal{D}[\cosh(r)\hat{a} + \sinh(r)\hat{a}^\dagger] \hat{\rho} \\ &\quad + \kappa_{\text{int}} \mathcal{D}[\hat{a}] \hat{\rho} + \frac{\gamma_\phi}{2} \sum_k \mathcal{D}[\hat{\sigma}_z^{(k)}] \hat{\rho} + \gamma_{\text{rel}} \sum_k \mathcal{D}[\hat{\sigma}_-^{(k)}] \hat{\rho}. \end{aligned} \quad (9)$$

We have also included standard single-spin decay and dephasing dissipators (at rates  $\gamma_{\text{rel}}$  and  $\gamma_{\phi}$ , respectively).

At a heuristic level, the cavity serves as a transducer that allows the spins to inherit the squeezed fluctuations produced by the bosonic squeezed reservoir. As the squeezed reservoir is engineered, we will treat  $r$  and  $\kappa_{\text{sqz}}$  as tuneable parameters that can be optimized. In contrast, we will take the coupling  $g$  and the unwanted dissipation (*i.e.*,  $\kappa_{\text{int}}$ ,  $\gamma_{\phi}$ , and  $\gamma_{\text{rel}}$ ) to be fixed. This then motivates introducing single-spin cooperativities  $\eta_k$  and collective cooperativities  $\mathcal{C}_k$  via:

$$\mathcal{C}_k \equiv N \frac{4g^2}{\kappa_{\text{int}}\gamma_k} \equiv N\eta_k, \quad (10)$$

where  $k \in \{\phi, \text{rel}\}$ . The goal will be to understand the optimal squeezing possible for a fixed value of  $\mathcal{C}_k$ . As we show in Sec. IV, in the case where single-spin relaxation dominates over dephasing, the optimized dissipative scheme achieves steady-state squeezing scaling as  $\xi_R^2 \propto 1/\sqrt{\mathcal{C}_{\text{rel}}}$ . This is significantly better than the optimized transient OAT squeezing in this regime, which only scales as  $\xi_R^2 \propto 1/(\mathcal{C}_{\text{rel}})^{1/3}$  [35].

To connect our setup to the simpler quantum master equation (2), we consider the regime where the condition  $\sqrt{N}g \ll \kappa_{\text{int}} + \kappa_{\text{sqz}}$  holds, and we adiabatically eliminate the cavity  $\hat{a}$ . We obtain (see App. A)

$$\begin{aligned} \dot{\hat{\rho}} = & \Gamma \mathcal{D} \left[ \hat{\Sigma}[r] \right] \hat{\rho} + \gamma_{\text{coll}} \mathcal{D} \left[ \hat{S}_- \right] \hat{\rho} \\ & + \frac{\gamma_{\phi}}{2} \sum_k \mathcal{D} \left[ \hat{\sigma}_z^{(k)} \right] \hat{\rho} + \gamma_{\text{rel}} \sum_k \mathcal{D} \left[ \hat{\sigma}_-^{(k)} \right] \hat{\rho}, \quad (11) \end{aligned}$$

where we have defined

$$\Gamma = \frac{4g^2}{(\kappa_{\text{sqz}} + \kappa_{\text{int}})^2} \kappa_{\text{sqz}}, \quad (12)$$

and

$$\gamma_{\text{coll}} = \frac{4g^2}{(\kappa_{\text{sqz}} + \kappa_{\text{int}})^2} \kappa_{\text{int}}. \quad (13)$$

We see that the internal loss of the cavity results in a collective relaxation process for the spin ensemble; this is similar to OAT-based protocols that are derived using a strongly detuned cavity-spin ensemble system (in contrast to the resonant regime considered here).

### III. THE EVEN-ODD EFFECT

#### A. Basic effect

A striking feature of the purely dissipative dynamics described by Eq. (2) is an extreme sensitivity to

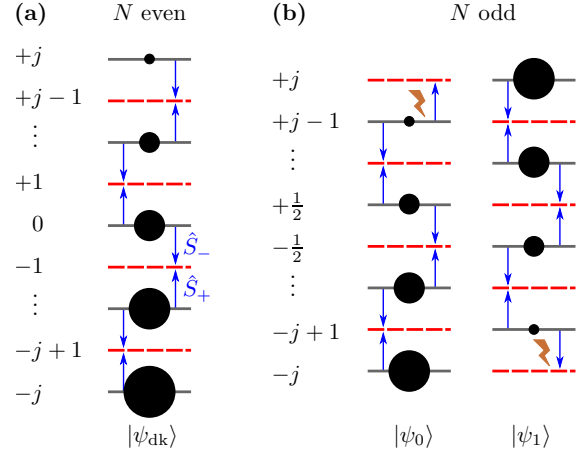


FIG. 2. Sketch of the steady state for (a) even  $N$  and (b) odd  $N$ . The size of the black circles represents the population of a level  $|j, m\rangle$ . For even  $N$ , a pure dark state exists for any squeezing parameter  $r$  because the jump operator  $\hat{\Sigma}$  leads to destructive interference between adjacent levels (blue arrows) such that every second level is unoccupied (dashed red lines). For odd  $N$  and large  $r$ , the interference condition cannot be satisfied for all levels (brown flashes) and the steady state is mixed. The two pure-state contributions with largest statistical weight are sketched here.

the parity of the number  $N$  of spins. As we will see, the steady state can be macroscopically different for  $N$  spins vs.  $N + 1$  spins. While early work noted that the form of the steady state depends on parity [21, 22], subsequent studies on achievable squeezing focused on the even- $N$  case [23, 25]. Our work reveals important new aspects of this parity effect. We show that by appropriate parameter tuning, one can avoid this effect, allowing steady-state squeezing that is near Heisenberg limited regardless of the parity of  $N$ . We also discuss a different regime where the even-odd effect could be used for a new sensing modality based on the macroscopic sensitivity to spin-number parity. Crucially, we show that there is no long timescale associated with the emergence of this sensitivity to the addition or removal of a single spin. Note that the even-odd effect in dissipative spin squeezing has no counterpart in bosonic dissipative squeezing.

We start with a simple intuitive picture that explains why the steady state of Eq. (2) is so sensitive to the parity of  $N$ . Recall that pure bosonic squeezed states are fully paired: they are superpositions of states having even photon numbers only [36]. A similar structure holds in our spin problem. We can think of the fully polarized state  $|j, m = -j\rangle$  as being the “vacuum”, and a state  $|j, m = -j + q\rangle$  as having  $q$  excitations (*i.e.*,  $q$  flipped spins). We thus see directly from Eq. (7) that, like bosonic squeezed

states, the spin dark states  $|\psi_{\text{dk}}[j; r]\rangle$  also only involve even numbers of excitations  $q$ .

Formally, in both the bosonic and spin problem, this paired structure leads to destructive interference that makes the state dark. When  $\hat{\Sigma}[r]$  acts on a paired state, it creates a state having only *odd* number of excitations. For a given odd excitation number  $q_{\text{odd}}$ , achieving a dark state requires destructive interference between the two pathways leading to  $q_{\text{odd}}$ :  $\hat{S}_-$  could have acted on the state with  $(q_{\text{odd}} + 1)$  excitations, or  $\hat{S}_+$  could have acted on the state with  $(q_{\text{odd}} - 1)$  excitations. These destructive interference conditions can be directly used to derive the coefficients in Eq. (7) that determine  $|\psi_{\text{dk}}[j; r]\rangle$ . This structure is shown schematically in Fig. 2.

With this picture in mind, it is easy to see why we cannot have a pure dark state for odd  $N$ . In this case, the maximum number of excitations  $q_{\text{max}}$  is *odd*. As such, the needed destructive interference is impossible to achieve. Starting with a fully paired state, we can create a state with  $q_{\text{max}}$  excitations by acting with  $\hat{S}_+$  on  $|j, -j + (q_{\text{max}} - 1)\rangle$ . However, there is no complementary  $\hat{S}_-$  process, as there is no state with  $q_{\text{max}} + 1$  excitations. The best one can then do is to construct fully paired states that are only approximately dark due to this incomplete destructive interference [see Fig. 2(b)].

The net result of this “frustration” is dramatic: for  $N$  odd and large  $r$ , the dissipative steady state of Eq. (2) is impure and, moreover, exhibits no spin squeezing for large  $r$ . For odd  $N$ , the steady state squeezing diverges in the large- $r$  limit, while the purity tends asymptotically to  $1/3$ . This behaviour is shown explicitly in Fig. 3. One also sees that, for modest  $r$ , there is no appreciable even-odd effect: the odd- $N$  steady state is almost pure and has the same squeezing as the even  $N$  case. This also follows from our heuristic picture: for small enough  $r$ , there is very little probability to have a large number of “excitations”, and hence one is almost insensitive to the frustration resulting from the cut-off on maximum excitation number.

While our discussion has been focused on the ideal quantum master equation (2), the even-odd effect persists even in the presence of single spin relaxation and dephasing [as described by Eq. (11) in the limit  $\kappa_{\text{int}} \rightarrow 0$ ]. As discussed in App. D, observing the even-odd effect in the steady state requires the single-spin cooperativities  $\eta_{\text{rel}}$  and  $\eta_{\phi}$  defined in Eq. (10) to be order unity or larger.

Finally, we note that the even-odd effect discussed here is distinct from the sensitivity to parity exhibited by unitary evolution under a OAT Hamiltonian  $\hat{H}_{\text{OAT}} = \chi \hat{S}_x^2$  [37–39]. The unitary evolution generated by  $\hat{H}_{\text{OAT}}$  for a time  $\pi/2\chi$  maps the initially

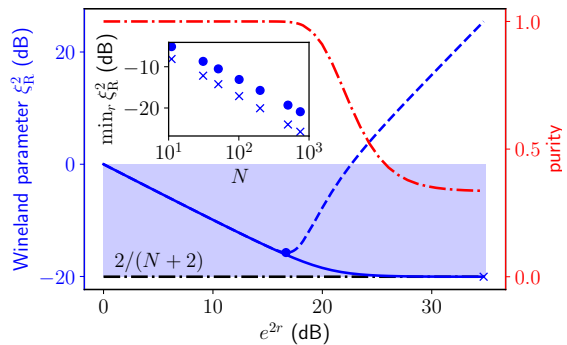


FIG. 3. Properties of the steady state of Eq. (2) for  $N = 200$  vs.  $N = 201$  spins. For even  $N$ , the Wineland parameter (solid blue line) converges to a Heisenberg-limited scaling (dash-dotted black line) in the limit  $r \rightarrow \infty$ . For odd  $N$ , the Wineland parameter (dashed blue line) diverges if  $e^{2r} \gg N$  and its purity (dash-dotted red line) approaches  $1/3$ . **Inset:** Minimum Wineland parameter for even  $N$  (crosses) and odd  $N$  (dots). The squeezed spin component is always  $\hat{S}_y$ .

fully polarized state  $|N/2, -N/2\rangle$  to Greenberger Horne Zeilinger (GHZ) states oriented along orthogonal axes in phase space, depending on the parity of  $N$ . This coherent effect results in a strong sensitivity to parity at a particular instant in time; in contrast, in our system, we have a dissipative effect where the sensitivity manifests itself in the *steady-state* of the system. Moreover, in our case, the even vs. odd states are not equivalent up to a rotation, but differ both in their purity and the magnitude of their fluctuations.

## B. Parity-independent Heisenberg-limited squeezing

In most experimental situations, the even-odd effect will be a nuisance: one aims for strong steady-state squeezing without needing to control  $N$  at the single particle level. We therefore derive a quantitative estimate on the maximum squeezing parameter  $r$  that can be used without any parity sensitivity. For small  $r$ , the system and its steady state are well described by a Holstein-Primakoff approximation [40]; one recovers bosonic squeezing physics [41], which is independent of the parity of  $N$ . However, the correspondence between bosonic squeezing and spin squeezing will break down if the populations of the states  $|j, m \approx j\rangle$  become nonzero. Using the steady-state occupation number of the Holstein-Primakoff bosons  $\langle \hat{b}^\dagger \hat{b} \rangle_{\text{ss}} = \sinh^2(r)$ , one can estimate that this breakdown happens if the condition

$\langle \hat{b}^\dagger \hat{b} \rangle_{\text{ss}} \approx N/2$  holds. This yields the breakdown criterion

$$e^{2r_{\text{crit}}} \gtrsim N, \quad (14)$$

which provides a good estimate for the maximum squeezing parameter  $r_{\text{crit}}$  possible with no even-odd effect.

While working with  $r \lesssim r_{\text{crit}}$  avoids parity effects, one might worry that this constraint precludes ever reaching Heisenberg-limited scaling of the steady-state spin squeezing. This is not the case. As shown in the inset of Fig. 3, the minimum Wineland parameter for odd  $N$  exhibits Heisenberg-like scaling, and the spin squeezing differs only by a constant prefactor  $\approx 2.6$  from the maximum achievable spin squeezing of  $\xi_R^2 = 2/(N+2)$  for even  $N$ .

### C. Connections to the LMG Model

Despite first appearances, the extreme even-odd effect of our system is more than a nuisance. At a fundamental level, the effect has a surprising connection to a seemingly unrelated closed-system many-body model, the LMG model [28]. To see this, recall that in a quantum trajectories formulation of the master equation in Eq. (2), the evolution of a state vector in the absence of quantum jumps is governed by the non-Hermitian Hamiltonian  $(-i/2)\hat{H}_{\text{LMG}}$ , where

$$\hat{H}_{\text{LMG}} \equiv \hat{\Sigma}^\dagger(r)\hat{\Sigma}(r) = e^{-2r}\hat{S}_x^2 + e^{2r}\hat{S}_y^2 + \hat{S}_z. \quad (15)$$

$\hat{H}_{\text{LMG}}$  is precisely the Hamiltonian of the anisotropic antiferromagnetic LMG model [28], a generalized transverse field Ising model with all-to-all Ising couplings.

Focusing on the case where  $N$  is odd and  $r > 0$ ,  $\hat{H}_{\text{LMG}}$  is positive and the steady state of Eq. (2) in a given total-angular-momentum subspace  $j$  can be written as (see App. D)

$$\hat{\rho}_{\text{ss}}^{(j)} = \frac{1}{\sum_{k=0}^{2j} \frac{1}{\lambda_k}} \sum_{k=0}^{2j} \frac{1}{\lambda_k} |\psi_k\rangle \langle \psi_k|, \quad (16)$$

where  $\lambda_k$  and  $|\psi_k\rangle$  are the ordered eigenvalues and eigenvectors of  $\hat{H}_{\text{LMG}}$ . We can thus directly connect the properties of the odd- $N$  steady state to the spectrum of the LMG Hamiltonian. Consider first the limit  $r \rightarrow 0$ , where  $\hat{H}_{\text{LMG}} \rightarrow \hat{S}^2 - \hat{S}_z^2 + \hat{S}_z$ . Then, the Hamiltonian has a *unique* ground state  $|\psi_0\rangle \rightarrow |\psi_{\text{dk}}[j;0]\rangle = |j, -j\rangle$ . Moreover, the ground-state energy is zero for any  $N$  and the gap to the double-degenerate first excited states is finite, *i.e.*,  $\lim_{r \rightarrow 0} \lambda_0 = 0$  and  $\lim_{r \rightarrow 0} \lambda_{1,2} = 2j$ . As a result,

the steady state is approximately pure even when  $N$  is odd, as  $|\psi_0\rangle$  dominates the sum in Eq. (16).

In the opposite limit  $r \rightarrow \infty$ , the LMG Hamiltonian is dominated by the  $\hat{S}_y^2$  term,  $\hat{H}_{\text{LMG}} \approx e^{2r}\hat{S}_y^2$ , and its eigenvalues are the eigenstates  $|j, m\rangle_y$  of  $\hat{S}_y$  with energy  $\lambda_m \approx m^2 e^{2r}$ . Now, there is no zero energy ground state for odd  $N$  (because  $m$  takes half-integer values), the ground state is double degenerate, and the steady state converges to an incoherent mixture of  $\hat{S}_y$  eigenstates,

$$\lim_{r \rightarrow \infty} \hat{\rho}_{\text{ss}}^{(j)} \propto \sum_{m=-j}^j \frac{1}{m^2} |j, m\rangle_y \langle j, m|. \quad (17)$$

A direct computation shows that the purity converges to  $\lim_{N \rightarrow \infty} \text{Tr}(\hat{\rho}_{\text{ss}}^{(N/2)}) = 1/3$ . In the limit  $r \rightarrow \infty$ , there is no mean spin polarization, but the variance of  $\hat{S}_y$  remains finite,  $\langle \hat{S}_y^2 \rangle \geq 1/4$ . As a result, the Wineland parameter will diverge as shown in Fig. 3.

The connection to the LMG model thus provides useful intuition into the odd- $N$  steady state. For even  $N$ , the dark state  $|\psi_{\text{dk}}[j;r]\rangle$  remains an exact zero mode of  $\hat{\Sigma}^\dagger(r)\hat{\Sigma}(r)$  for any value of  $r$  and interpolates smoothly between the limits  $|\psi_{\text{dk}}[j;0]\rangle = |j, -j\rangle$  and  $\lim_{r \rightarrow \infty} |\psi_{\text{dk}}[j;r]\rangle = |j, 0\rangle_y$ . In terms of the LMG model, this implies that for even  $N$ , the ground-state gap does not close as a function of  $r$  [42]. This feature of the LMG model has been discussed previously in the context of a *closed system* quantum phase transition [29, 43].

### D. Enhanced sensing

The dramatic even-odd sensitivity of the steady state enables a new kind of sensing modality: it provides a means for detecting changes in  $N$  at the single-spin level. This kind of sensing has long been of interest for both fundamental studies and applications [44–49]; a recent experiment has even used dispersive sensing to measure real-time changes in atom number in an atomic ensemble dispersively coupled to a cavity [50]. Our dissipative setup provides an alternative, potentially more powerful route for an analogous kind of sensing.

As discussed above, for a large squeezing parameter  $r \gg r_{\text{crit}}$ , the squeezing of the collective steady state depends exponentially on the parity of  $N$  (see Fig. 3). A simpler quantity, the variance of  $\hat{S}_y$ , also exhibits this strong sensitivity in the large  $r$  limit: for even  $N$ , it vanishes like  $N^2 e^{-4r}/8$  whereas, for odd  $N$ , it converges to the constant value  $N/\pi^2$  if  $N \gg 1$ . We thus see that measuring  $\hat{S}_y^2$  provides a direct means for estimating the parity of  $N$ . Such

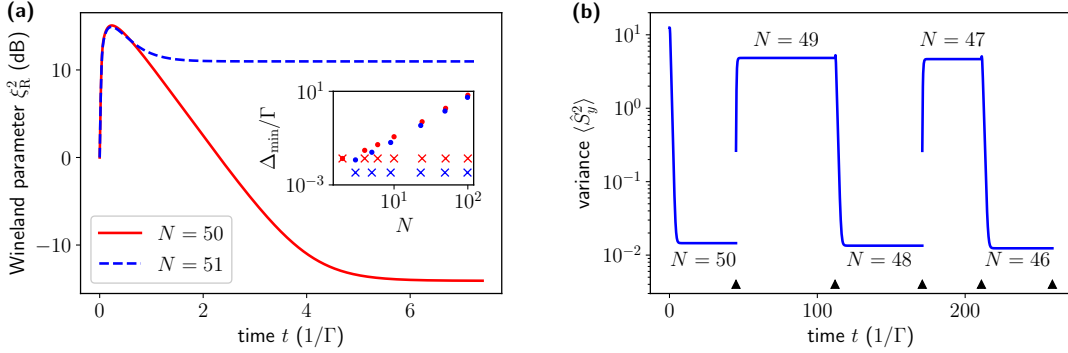


FIG. 4. **(a)** Time evolution of the coherent spin state  $|N/2, -N/2\rangle$  under the quantum master equation (2) for even vs. odd  $N$  with a squeezing parameter  $r = 2.5$ . **Inset:** Minimum spectral gap  $\Delta_{\min}$  of the Liouvillian associated with Eq. (2) in the maximum-angular-momentum subspace (points) and global minimum evaluated over all angular momentum subspaces (crosses). **(b)** Example of how the extreme even-odd sensitivity of the dissipative steady state could be used for sensing. The variance  $\langle \hat{S}_y^2 \rangle$  is plotted for a system described by the ideal quantum master equation (2) with  $r = 2.5$ , starting from the state  $|N/2, -N/2\rangle$ . The evolution is interrupted at randomly chosen times (black triangles), where a single (randomly chosen) spin is removed from the system. These spin-loss events cause the system to relax to a new steady state, leading to dramatic swings in the value of  $\langle \hat{S}_y^2 \rangle$  after each loss event. Note the logarithmic scale used for the  $y$  axis.

collective spin fluctuation measurements have been implemented in variety of systems [51–56].

While the parity sensitivity is in principle a steady-state effect, the relatively fast relaxation timescale here means that it can be harnessed for real-time sensing. We stress that the strong sensitivity to parity does not come at the expense of a vanishingly small bandwidth: if a spin is suddenly lost, the relaxation time to the new opposite-parity steady state is (at worst) set by the inverse coupling rate  $1/\Gamma$ . This timescale does not grow with system size [see inset of Fig. 4(a)]. The relaxation is even faster if one is in the maximum- $j$  subspace; here, the relaxation rate is collectively enhanced by a factor of  $N$ . We thus have a powerful means for detecting spins leaving or decoupling from the cavity one by one, as each such event causes a large change in  $\hat{S}_y^2$  [see Fig. 4(b), and App. D for more details]. The ability to detect spin or atom loss with this level of sensitivity could be leveraged to study a wide variety of physics. For example, one could use this for single photon detection, or to probe the many body physics of evaporation of cold atoms from a trap [50].

#### IV. ENHANCED PROTECTION AGAINST SINGLE-SPIN RELAXATION

The dissipative approach to spin squeezing also provides strong advantages when unwanted single-spin dissipation is included. In this section, we focus on the case where local relaxation is dominant, *i.e.*, we study Eq. (11) in the limit  $\gamma_{\text{rel}} \neq 0, \gamma_{\phi} \rightarrow 0$ .

For atomic systems, this can be viewed as a fundamental limit arising from spontaneous emission, whereas single-spin dephasing is a technical imperfection. As noted in Ref. 35, in this limit, standard OAT achieves an optimized squeezing that yields the scaling  $\xi_R^2 \sim C_{\text{rel}}^{-1/3}$  for large  $N$ . This work also introduced an alternate Hamiltonian protocol involving two mutually-interacting spin ensembles, which could achieve a more favourable  $\xi_R^2 \sim C_{\text{rel}}^{-1/2}$  scaling at a specific optimized time. As we show below, our dissipative approach can achieve an identical scaling, but now for the *steady state*, and only using a single ensemble of standard two-level systems. We also show that this enhanced performance over OAT holds even for small- $N$  ensembles. Note that single-spin dissipation was also studied in Ref. 25, but only for spontaneous emission in an ensemble of 4-level atoms with a specific structure. This is distinct from the more generic model Eq. (11) we study.

Focusing on the limit of large  $N$  and a small single-spin cooperativity, we can approximate our system well using a standard mean-field theory based on linearizing the equations of motion for the system’s covariance matrix. Solving these in the steady state and considering the limit of a sufficiently large  $r$  (see App. C), one finds that the steady-state squeezing is

$$\xi_R^2 \approx \frac{N\gamma_{\text{coll}} + \Gamma + \gamma_{\text{rel}}}{N\gamma_{\text{coll}} + \Gamma N + \gamma_{\text{rel}}}. \quad (18)$$

The numerator here describes unwanted heating by both single-spin relaxation and the collective decay

$\gamma_{\text{coll}}$  associated with internal cavity loss. The only parameter left to optimize over is  $\kappa_{\text{sqz}}$ , the coupling between the cavity and the squeezed reservoir, which enters Eq. (18) via Eqs. (12) and (13). There is a non-trivial minimum here. Suppression of unwanted collective heating requires a large  $\kappa_{\text{sqz}}$ , as this reduces the ratio  $\gamma_{\text{coll}}/\Gamma$ . In contrast, suppressing the effects of  $\gamma_{\text{rel}}$  requires a large  $\Gamma$  and hence small  $\kappa_{\text{sqz}}$ .

Minimizing with respect to  $\kappa_{\text{sqz}}$ , we find

$$\xi_R^2 \approx \frac{2}{\sqrt{c_{\text{rel}}}} + \mathcal{O}\left(\frac{1}{c_{\text{rel}}}\right), \quad (19)$$

where the optimal value of  $\kappa_{\text{sqz}}$  satisfies

$$\kappa_{\text{sqz}}^{\text{opt}} = \kappa_{\text{int}} \sqrt{c_{\text{rel}}} + \mathcal{O}(c_{\text{rel}}^0). \quad (20)$$

We thus obtain an optimized squeezing that scales significantly better with collective cooperativity in this relaxation-dominated regime than the OAT result of  $\xi_R^2 \sim c_{\text{rel}}^{-1/3}$ . In App. C2 we show numerical simulations of a more accurate non-linear mean-field theory that confirm these results. As we have stressed, the squeezing here is also achieved in the steady state (and not just at one optimal time). While we assumed a large value of  $r$  to derive these results, in practice one only needs  $\exp(-2r) \ll 1/\sqrt{c_{\text{rel}}}$  for this scaling to hold.

The advantage over OAT in this relaxation-dominated regime also persists for smaller-sized spin ensembles. To study this regime, we numerically solve Eq. (11) for the steady state. Figure 5 shows the obtained results for the steady state squeezing (orange curve) as a function of  $N$ , where we have fixed  $g$ ,  $\kappa_{\text{int}}$ , and  $\gamma_{\text{rel}}$  so that the single-spin cooperativity is  $\eta_{\text{rel}} = 2$ . For each value of  $N$ , we optimize the parameters of the squeezed reservoir ( $\kappa_{\text{sqz}}, r$ ) to minimize the steady state  $\xi_R^2$ ; the optimized values are presented in App. F. For comparison, we also plot the optimized *transient* squeezing achievable using OAT (blue curve) in an identical cavity-spin system [27, 35] (see App. G for details). For the OAT setup, there is no squeezed reservoir,  $\kappa_{\text{sqz}} = 0$ , and there is a large detuning  $\Delta$  between the spins and cavity, which is optimized for each value of  $N$ .

Figure 5 shows that, even for small  $N$ , the dissipative protocol yields an advantage over OAT. While for these small values of  $N$  and large  $\eta_{\text{rel}}$ , the linearized mean-field theory scaling predictions are not expected to hold exactly, there is a qualitative agreement with the predicted powerlaws (as indicated by black dashed lines).

In App. H, we provide a brief performance analysis of a special case where  $\kappa_{\text{int}} = 0$ . Mathematically, such a scenario is equivalent to a setup where one directly shines squeezed light onto the spin ensemble. We show that in the limit of large spin number,

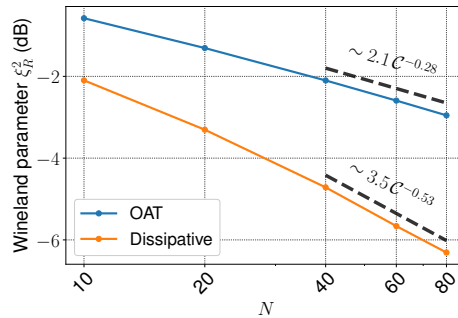


FIG. 5. A comparison of the Wineland parameter  $\xi_R^2$  between the dissipative (blue) and OAT (orange) protocols with as a function of  $N$  for a small number of spins. The simulations have been performed by evolving the spin-only quantum master equation [see Eq. (11) for the case of dissipative protocol, and App. G for the details on OAT]. In the dissipative protocol, at each value of  $N$ , both  $r$  as well as  $\kappa_{\text{sqz}}$  have been optimized, while in the case of OAT, the optimization has been performed over the cavity-spin detuning. The parameters used in both cases are  $\gamma_{\text{rel}} = 0.02g$  and  $\kappa_{\text{int}} = 100g$ , resulting in single spin cooperativity of  $\eta_{\text{rel}} = 2$ . The two dashed lines show fits of the last few data points.

one can achieve the scaling of  $\xi_R^2 \propto (N\Gamma/\gamma_{\text{rel}})^{-1}$ , although naturally, having either  $\kappa_{\text{int}} = 0$  or irradiating a spin ensemble directly, would likely be difficult to realize experimentally.

## V. DEPHASING-DOMINATED REGIME: PRE-THERMALIZATION AND EMERGENT SLOW TIMESCALES

We now consider the effects of weak single-spin dephasing [*i.e.*, the  $\gamma_\phi$  term in Eq. (11)] on our dissipative spin squeezing protocol. For very weak dephasing, such that  $\gamma_\phi < \gamma_{\text{rel}}/N$  holds, the mean-field theory results of the previous section still provide a good description; one simply substitutes  $\gamma_{\text{rel}} \rightarrow \gamma_{\text{rel}} + 2\gamma_\phi$  in Eqs. (19) and (20). The more interesting case is when dephasing is the dominant form of single-spin dissipation, but is still weak compared to the rate  $\Gamma$  associated with the collective spin squeezing dissipator (*i.e.*,  $\Gamma \gg \gamma_\phi \gg \gamma_{\text{rel}}$ ). In this case, the dynamics is surprisingly rich, exhibiting features reminiscent of prethermalization behavior observed in weakly nonintegrable systems [30, 31]. Prethermalization is associated with approximately conserved quantities that can only be dynamically randomized on extremely long timescales; this results in an intermediate-time quasi-steady state whose form is contingent on the initial value of the conserved quan-



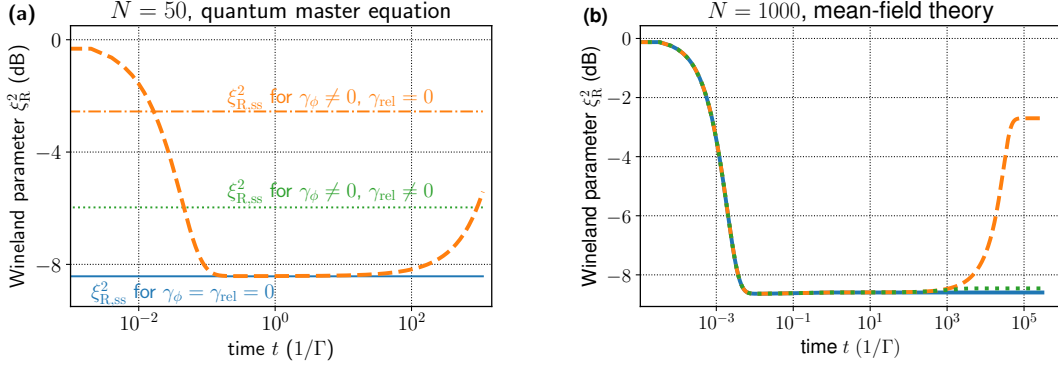


FIG. 6. Time evolution of the Wineland spin squeezing parameter  $\xi_R^2$  in the presence of local dissipation (note the logarithmic scale of the time axis). **(a)** Wineland parameter calculated using the quantum master equation (11) for weak local dephasing and  $N = 50$  spins (thick dashed orange line,  $\gamma_\phi/\Gamma = 0.005$ ,  $\gamma_{\text{rel}}/\Gamma = 0$ , and  $\gamma_{\text{coll}}/\Gamma = 0$ ). The final amount of steady-state spin squeezing is indicated by the thin dash-dotted orange line. Local dephasing deteriorates the amount of steady-state spin squeezing compared to an ideal system without local dissipation (solid blue line,  $\gamma_\phi/\Gamma = \gamma_{\text{rel}}/\Gamma = \gamma_{\text{coll}}/\Gamma = 0$ ). Local relaxation counteracts this effect and partially restores the steady-state spin squeezing (dotted green line,  $\gamma_\phi/\Gamma = 0.005$ ,  $\gamma_{\text{rel}}/\Gamma = 0.001$ , and  $\gamma_{\text{coll}}/\Gamma = 0$ ). Note that the *transient* state is strongly spin squeezed even in the presence of local dissipation since the collective dissipator  $\hat{\Sigma}$  induces spin squeezing on a short timescale  $\propto 1/N\Gamma$  whereas the system approaches its steady state on a longer system-size-dependent timescale  $\propto N/\gamma_\phi$ . **(b)** Wineland parameter calculated using the mean-field equations of motion detailed in App. B for  $N = 1000$  spins and the same sets of dissipation rates as in (a).

ties. Here, a similar phenomenon arises, with total angular momentum playing the role of the approximately conserved quantity. We discuss this more in what follows.

Starting from an initial product state, we find that a seemingly tiny amount of single-spin dephasing is enough to completely destroy spin squeezing in the eventual steady state. Using a mean-field analysis, one can show that in the presence of arbitrarily weak but non-zero single-spin dephasing (and  $\gamma_{\text{rel}} = \gamma_{\text{coll}} = 0$ ), the steady state squeezing is bounded by  $-3$  dB in the large  $N$  limit:

$$\lim_{\gamma_\phi \rightarrow 0} \xi_R^2 \geq \frac{1}{2} + \frac{\sqrt{N}}{N+1}, \quad (21)$$

where the optimal value is achieved with  $r = \frac{1}{8} \ln N$ .

Despite this, there exists an extremely long-lived intermediate-time regime (a quasi-steady state) where strong spin squeezing is observed. The system’s dissipative dynamics is thus characterized by two vastly different timescales, as shown in Fig. 6. The system first evolves into a transient spin squeezed state on a fast timescale  $\propto 1/N\Gamma$ . In contrast, the eventual relaxation to the true steady state (which has minimal squeezing) occurs on a much slower timescale  $\propto N/\gamma_\phi$ . For a large system size  $N$ , the ratio of these timescales can be dramatic. We also note that the slow relaxation time is parametrically slower than the single-spin dephasing time  $1/\gamma_\phi$ .

The emergence of this surprisingly long timescale, and the corresponding fragility of the steady state to weak dephasing, are both surprising; we stress that single-spin relaxation (as discussed in the previous section) does not give rise to an analogous behavior. In App. E, we analyze this effect using Liouvillian perturbation theory [57] and use it to provide an intuitive physical picture: Single-spin dephasing enables transitions between subspaces of different total angular momentum [34] such that an initial state in the  $j = j_{\text{max}}$  subspace evolves into a steady state populating subspaces with  $j < j_{\text{max}}$ . The degeneracy of the  $j < j_{\text{max}}$  subspaces gives rise to anomalously small matrix elements between the subspaces, which represent bottlenecks for the relaxation to the steady state.

We stress that the surprising impact of dephasing need not be problematic for experiments. The spin squeezing exhibited by the Wineland parameter  $\xi_R^2$  in the “prethermalized” intermediate-time regime is comparable to  $\xi_R^2$  of the steady state obtained in an *ideal* system without single-spin dissipation, as long as the conditions  $\gamma_\phi \ll \Gamma, N\gamma_\phi$  are satisfied. Moreover, there is a simple but effective way to improve the spin squeezing of the steady state by deliberately adding a competing single-spin relaxation process  $\gamma_{\text{rel}}$ . If this relaxation rate satisfies the condition  $\gamma_{\text{rel}} \gtrsim \gamma_\phi/N$ , population will be pushed back to the large-angular-momentum subspaces, which decreases the steady-state Wineland parameter significantly and increases spin squeezing

beyond the  $-3$  dB limit, as shown in Fig. 6.

## VI. HYBRID-SYSTEMS IMPLEMENTATION USING DISSIPATIVE BOSONIC SQUEEZING

As discussed in Sec. II B, the dissipative spin squeezing setup described by the general quantum master equation in Eq. (11) can be realized using standard two-level systems (unlike the more structured four-level atoms in Refs. [9, 25]), and *without* requiring the use of non-classical squeezed input light. Instead, one harnesses a standard (resonant) Tavis–Cummings coupling between a spin ensemble and a bosonic mode, along with the dissipative squeezing of this bosonic mode. The second element here has been experimentally realized in a variety of systems. In this section, we provide more details on the physical implementation of our hybrid-systems approach to dissipative spin squeezing in three promising platforms: trapped ions, solid-state optomechanical devices, and superconducting circuits.

### A. Trapped ions

In trapped ions, the relevant spin degree of freedom usually corresponds to two metastable internal states (spin or orbital) of each individual ion. In contrast, the bosonic “cavity” mode corresponds to a collective motional mode of the ions [58]. Recent experiments have already utilized the spin-motion coupling for over 50 ions in a 2D Penning trap [54] and 1D linear Paul trap [59]. The desired Tavis–Cummings coupling is commonly realized by applying a laser field that is resonant with the red motional sideband of the spin-level transition (see, *e.g.*, Ref. 60). Motional dissipation is, in turn, mediated by coupling the motional mode to a dipole-allowed transition of an ion. To realize dissipative spin squeezing with  $N$  spins, we imagine a setup that consists of  $N + 1$  ions.  $N$  of these ions make up the spin ensemble that we wish to squeeze; the remaining additional ion serves as a “cooler” ion that is used to dissipatively squeeze the collective motional mode. A squeezed bath can be engineered by applying two laser fields that are resonant with the red and blue sideband transitions of the cooler ion [12], leading to an effective Hamiltonian

$$\hat{H}_{\text{ion}} = G_{\text{ion}}^{(-)} \hat{a}^\dagger \hat{\sigma}_- + G_{\text{ion}}^{(+)} \hat{a} \hat{\sigma}_- + \text{h. c.}, \quad (22)$$

where  $G_{\text{ion}}^{(-)}$  ( $G_{\text{ion}}^{(+)}$ ) is the red (blue) sideband coupling, and  $\hat{\sigma}_-$  is the lowering operator of the cooler-

ion transition. The squeezing strength can be controlled by the ratio of the couplings, *i.e.*,  $\tanh(r) = |G_{\text{ion}}^{(+)} / G_{\text{ion}}^{(-)}|$ , and the squeezed axis is determined by their relative phase. Such engineered squeezed dissipation has recently been utilized to dissipatively prepare a motional state with over  $-12$  dB of squeezing [16]. Our scheme allows this dissipative phononic squeezing to now enable metrologically-useful dissipative spin squeezing.

### B. Solid-state spins in an optomechanical crystal

In solid-state platforms, the spin ensemble in our scheme could be realized using defect centers in a semiconductor, *e.g.*, NV-center defect spins in diamond. These spins can be implanted in a structure which in turn realizes an optomechanical crystal: a patterned photonic crystal beam with a defect that localizes both a mechanical mode and an optical mode [61]. We note that high-Q diamond optomechanical crystals have been realized experimentally [62], with a recent experiment even integrating such a system with NV center defect spins [63]. The localized mechanical mode plays the role of the bosonic “cavity” in Eq. (11). The spins and mechanical motion exhibit an intrinsic coupling due to the strain dependence of spin level transitions, and the coupling could be further enhanced by incorporating the high strain sensitivity of excited states through phonon-assisted Raman transitions [63–65].

In this kind of setup, the optomechanical coupling between the localized mechanical and optical cavity mode provides a mechanism for the dissipative squeezing of the mechanical mode. If one is in the sideband resolved regime (where the mechanical frequency is larger than the optical cavity decay rate), then this dissipative mechanical squeezing can be realized by driving the optical cavity by two control lasers that are resonant to the red and blue motional sidebands, respectively [41]. We stress these are classical, coherent state drives. Ignoring the non-linear coupling that is usually negligibly weak in most platforms, the optomechanical coupling is well approximated by

$$\hat{H}_{\text{OM}} = G_{\text{OM}}^{(-)} \hat{a}^\dagger \hat{b} + G_{\text{OM}}^{(+)} \hat{a} \hat{b} + \text{h. c.}, \quad (23)$$

where  $G_{\text{OM}}^{(-)}$  ( $G_{\text{OM}}^{(+)}$ ) is the red (blue) sideband optomechanical coupling strength, and  $\hat{b}$  is the annihilation operator of the optical cavity mode. The squeezing strength is determined by the ratio of the red and blue sideband coupling, *i.e.*,  $\tanh(r) = |G_{\text{OM}}^{(+)} / G_{\text{OM}}^{(-)}|$ , which can be tuned by varying the amplitude of the driving tones. We note that this kind

of dissipative squeezing of mechanical motion via optomechanics has been realized in several experiments [15, 17–19]. Our protocol thus provides a means of harnessing this capability to generate spin squeezing. Finally, in solid-state settings inhomogeneous broadening of the spin ensemble is almost always an issue; this is typically mitigated by using dynamical decoupling techniques. By using the ability to control the bosonic squeezing in time (*e.g.*, via the amplitude of the sideband drives) our protocol can be made compatible with simultaneous dynamical decoupling of this spins.

### C. Superconducting microwave cavities

Superconducting microwave cavities and circuit QED are another promising class of systems for implementing our ideas. Our basic building block of a bosonic mode coupled to a spin ensemble could be realized by coupling a single microwave cavity mode to either a set of superconducting qubits [66–69], or to electronic spins in substrate (*e.g.*, Bi donors implanted in Si [70, 71]). The second ingredient, a mechanism for the dissipative generation of microwave squeezing, could also be implemented in different ways. One approach is to inject squeezed microwave radiation directly into the cavity using the output of a Josephson parametric amplifier [72–74]. This has already been achieved experimentally in Ref. 70, in a system where a cavity has been coupled to a spin ensemble. An alternate approach which has the advantage of not being limited by insertion losses (associated with transporting a squeezed state) is to mimic the same dissipative squeezing protocols used in optomechanics to squeeze a mechanical mode. This can be accomplished by coupling three microwave modes via a Josephson ring modulator [75], which generates a three-wave mixing term  $(\hat{p} + \hat{p}^\dagger)(\hat{a} + \hat{a}^\dagger)(\hat{b} + \hat{b}^\dagger)$  between the modes  $\hat{a}$ ,  $\hat{b}$ , and  $\hat{p}$  [76]. By driving the pump mode  $\hat{p}$  coherently at the sum and difference frequency of the  $\hat{a}$  and  $\hat{b}$  modes,  $\omega_\pm$ , one can engineer an interaction of the form of Eq. (23), where the prefactors  $G_{\text{OM}}^{(\pm)}$  depend on the strength of the drives at  $\omega_\pm$ , respectively. Adiabatic elimination of the strongly-damped  $\hat{b}$  mode generates an effective squeezed bath for the  $\hat{a}$  mode as shown in Eq. (9). A recent experiment implementing this approach has demonstrated up to  $-8$  dB of intracavity squeezing of the  $\hat{a}$  mode [20].

## VII. CONCLUSIONS

In this work, we have revisited the reservoir-engineering approach to preparing and stabilizing spin-squeezed states. We analyzed in detail a particular implementation strategy that had not previously been studied, but that is compatible with a number of experimental platforms: employ a hybrid-systems approach where one first uses bosonic reservoir-engineering techniques to stabilize a bosonic squeezed state, and then uses this state (via a standard Tavis-Cummings-type coupling) to dissipatively squeeze a spin ensemble. We also discussed how this approach compared favourably to the standard one-axis twist method for spin squeezing in the presence of single-spin relaxation.

Our work also addressed fundamental aspects of dissipative spin squeezing, with a focus on two general but surprising phenomena. The first was an extreme, macroscopic sensitivity of the steady state to the parity of the number  $N$  of spins in the ensemble. We analyzed both how this effect could be avoided (if the goal was to generate spin squeezing without any parity sensitivity), and how it might be harnessed for a powerful new sensing modality. The second general effect we studied was the emergence of a surprisingly long slow timescale and “prethermalization” behavior when weak single-spin dephasing is added to our model. While the steady state in this regime exhibits at best limited squeezing, the intermediate time quasi-steady state can be highly squeezed. Moreover, the reduction of steady-state spin squeezing can be almost completely suppressed by deliberately introducing a small amount of single-spin relaxation.

We hope our work will lay the groundwork for near-term experimental implementations of reservoir-engineered spin squeezing in a variety of systems. In future theoretical work, it will be interesting to explore extensions of the models analyzed here. For example, it is well known that collective Hamiltonian interactions that are not truly infinite range can still generate large amounts of spin squeezing [77, 78]. Is the same true with dissipative spin-spin interactions, and if so, are the requirements more or less forgiving than in the coherent case? It would also be interesting to study in more detail the effects of disorder, *e.g.*, due to inhomogeneous broadening, both on spin squeezing and on the parity-sensing scheme proposed here.

## ACKNOWLEDGEMENTS

This work was primarily supported by the DARPA DRINQS program (agreement D18AC00014). We

also acknowledge partial support by the University of Chicago Materials Research Science and Engineer-

ing Center, which is funded by the National Science Foundation under Grant No. DMR-1420709. We thank A.-M. Rey and M. Kloc for useful discussions.

- 
- [1] M. Kitagawa and M. Ueda, *Phys. Rev. A* **47**, 5138 (1993).
- [2] L. Pezzè, A. Smerzi, M. K. Oberthaler, R. Schmied, and P. Treutlein, *Rev. Mod. Phys.* **90**, 035005 (2018).
- [3] I. D. Leroux, M. H. Schleier-Smith, and V. Vuletić, *Phys. Rev. Lett.* **104**, 073602 (2010).
- [4] M. F. Riedel, P. Böhi, Y. Li, T. W. Hänsch, A. Sinatra, and P. Treutlein, *Nature* **464**, 1170 (2010).
- [5] C. Gross, T. Zibold, E. Nicklas, J. Estève, and M. K. Oberthaler, *Nature* **464**, 1165 (2010).
- [6] O. Hosten, R. Krishnakumar, N. J. Engelsen, and M. A. Kasevich, *Science* **352**, 1552 (2016).
- [7] P. Cappellaro and M. D. Lukin, *Phys. Rev. A* **80**, 032311 (2009).
- [8] Y. C. Liu, Z. F. Xu, G. R. Jin, and L. You, *Phys. Rev. Lett.* **107**, 013601 (2011).
- [9] J. Borregaard, E. Davis, G. S. Bentsen, M. H. Schleier-Smith, and A. S. Sørensen, *New J. Phys.* **19**, 093021 (2017).
- [10] P. Groszkowski, H.-K. Lau, C. Leroux, L. Govia, and A. Clerk, *Physical Review Letters* **125**, 203601 (2020).
- [11] J. F. Poyatos, J. I. Cirac, and P. Zoller, *Phys. Rev. Lett.* **77**, 4728 (1996).
- [12] J. I. Cirac, A. S. Parkins, R. Blatt, and P. Zoller, *Physical Review Letters* **70**, 556 (1993).
- [13] A. Kronwald, F. Marquardt, and A. A. Clerk, *Phys. Rev. A* **88**, 063833 (2013).
- [14] N. Didier, F. Qassemi, and A. Blais, *Physical Review A* **89**, 013820 (2014).
- [15] E. E. Wollman, C. U. Lei, A. J. Weinstein, J. Suh, A. Kronwald, F. Marquardt, A. A. Clerk, and K. C. Schwab, *Science* **349**, 952 (2015).
- [16] D. Kienzler, H.-Y. Lo, B. Keitch, L. d. Clercq, F. Lepold, F. Lindenfesler, M. Marinelli, V. Negnevitsky, and J. P. Home, *Science* **347**, 53 (2015).
- [17] F. Lecocq, J. B. Clark, R. W. Simmonds, J. Aumentado, and J. D. Teufel, *Phys. Rev. X* **5**, 041037 (2015).
- [18] J.-M. Pirkkalainen, E. Damskägg, M. Brandt, F. Massel, and M. A. Sillanpää, *Phys. Rev. Lett.* **115**, 243601 (2015).
- [19] C. U. Lei, A. J. Weinstein, J. Suh, E. E. Wollman, A. Kronwald, F. Marquardt, A. A. Clerk, and K. C. Schwab, *Phys. Rev. Lett.* **117**, 100801 (2016).
- [20] R. Dassonneville, R. Assouly, T. Peronnin, A. A. Clerk, A. Bienfait, and B. Huard, *arXiv preprint* (2021), 2102.02863v1.
- [21] G. S. Agarwal and R. R. Puri, *Optics Communications* **69**, 267 (1989).
- [22] G. S. Agarwal and R. R. Puri, *Phys. Rev. A* **41**, 3782 (1990).
- [23] G. S. Agarwal and R. R. Puri, *Phys. Rev. A* **49**, 4968 (1994).
- [24] A. Kuzmich, K. Mølmer, and E. S. Polzik, *Phys. Rev. Lett.* **79**, 4782 (1997).
- [25] E. G. Dalla Torre, J. Otterbach, E. Demler, V. Vuletic, and M. D. Lukin, *Phys. Rev. Lett.* **110**, 120402 (2013).
- [26] M. Tavis and F. W. Cummings, *Phys. Rev.* **170**, 379 (1968).
- [27] S. D. Bennett, N. Y. Yao, J. Otterbach, P. Zoller, P. Rabl, and M. D. Lukin, *Phys. Rev. Lett.* **110**, 156402 (2013).
- [28] H. Lipkin, N. Meshkov, and A. Glick, *Nuclear Physics* **62**, 188 (1965).
- [29] R. G. Unanyan and M. Fleischhauer, *Phys. Rev. Lett.* **90**, 133601 (2003).
- [30] L. D’Alessio, Y. Kafri, A. Polkovnikov, and M. Rigol, *Advances in Physics* **65**, 239 (2016).
- [31] T. Langen, T. Gasenzer, and J. Schmiedmayer, *Journal of Statistical Mechanics: Theory and Experiment* **2016**, 064009 (2016).
- [32] D. J. Wineland, J. J. Bollinger, W. M. Itano, F. Moore, and D. Heinzen, *Physical Review A* **46**, R6797 (1992).
- [33] R. H. Dicke, *Phys. Rev.* **93**, 99 (1954).
- [34] B. A. Chase and J. M. Geremia, *Phys. Rev. A* **78**, 052101 (2008).
- [35] R. J. Lewis-Swan, M. A. Norcia, J. R. K. Cline, J. K. Thompson, and A. M. Rey, *Phys. Rev. Lett.* **121**, 070403 (2018).
- [36] C. Gerry and P. Knight, *Introductory Quantum Optics* (Cambridge University Press, Cambridge, 2005).
- [37] K. Mølmer and A. Sørensen, *Phys. Rev. Lett.* **82**, 1835 (1999).
- [38] D. Leibfried, M. D. Barrett, T. Schaetz, J. Britton, J. Chiaverini, W. M. Itano, J. D. Jost, C. Langer, and D. J. Wineland, *Science* **304**, 1476 (2004).
- [39] D. Leibfried, E. Knill, S. Seidelin, J. Britton, R. B. Blakestad, J. Chiaverini, D. B. Hume, W. M. Itano, J. D. Jost, C. Langer, R. Ozeri, R. Reichle, and D. J. Wineland, *Nature* **438**, 639 (2005).
- [40] T. Holstein and H. Primakoff, *Phys. Rev.* **58**, 1098 (1940).
- [41] A. Kronwald, F. Marquardt, and A. A. Clerk, *New Journal of Physics* **16**, 063058 (2014).
- [42] R. G. Unanyan, *Theoretical and Mathematical Physics* **195**, 718 (2018).
- [43] R. G. Unanyan, C. Ionescu, and M. Fleischhauer, *Phys. Rev. A* **72**, 022326 (2005).
- [44] J. McKeever, J. R. Buck, A. D. Boozer, and H. J. Kimble, *Phys. Rev. Lett.* **93**, 143601 (2004).
- [45] I. Teper, Y.-J. Lin, and V. Vuletić, *Phys. Rev. Lett.* **97**, 023002 (2006).

- [46] K. M. Fortier, S. Y. Kim, M. J. Gibbons, P. Ahmadi, and M. S. Chapman, *Phys. Rev. Lett.* **98**, 233601 (2007).
- [47] N. Brahms, T. P. Purdy, D. W. C. Brooks, T. Botter, and D. M. Stamper-Kurn, *Nature Physics* **7**, 604 (2011).
- [48] H. Zhang, R. McConnell, S. Ćuk, Q. Lin, M. H. Schleier-Smith, I. D. Leroux, and V. Vuletić, *Phys. Rev. Lett.* **109**, 133603 (2012).
- [49] Z. Chen, J. G. Bohnet, J. M. Weiner, K. C. Cox, and J. K. Thompson, *Phys. Rev. A* **89**, 043837 (2014).
- [50] J. Zeiher, J. Wolf, J. A. Isaacs, J. Kohler, and D. M. Stamper-Kurn, *arXiv preprint* (2020), 2012.01280.
- [51] J. Appel, P. J. Windpassinger, D. Oblak, U. B. Hoff, N. Kjærgaard, and E. S. Polzik, *Proceedings of the National Academy of Sciences* **106**, 10960 (2009).
- [52] T. Takano, M. Fuyama, R. Namiki, and Y. Takahashi, *Phys. Rev. Lett.* **102**, 033601 (2009).
- [53] M. H. Schleier-Smith, I. D. Leroux, and V. Vuletić, *Phys. Rev. Lett.* **104**, 073604 (2010).
- [54] J. G. Bohnet, B. C. Sawyer, J. W. Britton, M. L. Wall, A. M. Rey, M. Foss-Feig, and J. J. Bollinger, *Science* **352**, 1297 (2016).
- [55] J.-B. Béguin, J. H. Müller, J. Appel, and E. S. Polzik, *Phys. Rev. X* **8**, 031010 (2018).
- [56] V. Guarrera, R. Gartman, G. Bevilacqua, and W. Chalupczak, *arXiv preprint* (2020), 2012.12617v1.
- [57] A. C. Y. Li, F. Petruccione, and J. Koch, *Scientific Reports* **4**, 4887 (2014).
- [58] H. Häffner, C. F. Roos, and R. Blatt, *Physics Reports* **469**, 155 (2008).
- [59] J. Zhang, G. Pagano, P. W. Hess, A. Kyprianidis, P. Becker, H. Kaplan, A. V. Gorshkov, Z. X. Gong, and C. Monroe, *Nature* **551**, 601 (2017).
- [60] D. Porras and J. I. Cirac, *Physical Review Letters* **92**, 207901 (2004).
- [61] M. Eichenfield, J. Chan, R. M. Camacho, K. J. Vahala, and O. Painter, *Nature* **462**, 78 (2009).
- [62] M. J. Burek, J. D. Cohen, S. M. Meenehan, N. El-Sawah, C. Chia, T. Ruelle, S. Meesala, J. Rochman, H. A. Atikian, M. Markham, D. J. Twitchen, M. D. Lukin, O. Painter, and M. Lončar, *Optica* **3**, 1404 (2016).
- [63] J. V. Cady, O. Michel, K. W. Lee, R. N. Patel, C. J. Sarabalis, A. H. Safavi-Naeini, and A. C. Bleszynski Jayich, *Quantum Science and Technology* **4**, 024009 (2019).
- [64] D. A. Golter, T. Oo, M. Amezcua, K. A. Stewart, and H. Wang, *Physical Review Letters* **116**, 143602 (2016).
- [65] A. Albrecht, A. Retzker, F. Jelezko, and M. Plenio, *New Journal of Physics* **15**, 083014 (2013).
- [66] P. Macha, G. Oelsner, J.-M. Reiner, M. Marthaler, S. André, G. Schön, U. Hübner, H.-G. Meyer, E. Il'ichev, and A. V. Ustinov, *Nature Communications* **5**, 1 (2014).
- [67] K. V. Shulga, P. Yang, G. P. Fedorov, M. V. Fistul, M. Weides, and A. V. Ustinov, *JETP Letters* **105**, 47 (2017).
- [68] C. Song, K. Xu, H. Li, Y.-R. Zhang, X. Zhang, W. Liu, Q. Guo, Z. Wang, W. Ren, J. Hao, H. Feng, H. Fan, D. Zheng, D.-W. Wang, H. Wang, and S.-Y. Zhu, *Science* **365**, 574 (2019).
- [69] J. D. Brehm, A. N. Poddubny, A. Stehli, T. Wolz, H. Rotzinger, and A. V. Ustinov, *npj Quantum Materials* **6**, 10 (2021).
- [70] A. Bienfait, P. Campagne-Ibarcq, A. H. Kiilerich, X. Zhou, S. Probst, J. J. Pla, T. Schenkel, D. Vion, D. Esteve, J. J. L. Morton, K. Mølmer, and P. Bertet, *Phys. Rev. X* **7**, 041011 (2017).
- [71] B. Albanese, S. Probst, V. Ranjan, C. W. Zollitsch, M. Pechal, A. Wallraff, J. J. L. Morton, D. Vion, D. Esteve, E. Flurin, and P. Bertet, *Nature Physics* **16**, 751 (2020).
- [72] M. A. Castellanos-Beltran, K. D. Irwin, G. C. H. van L R Vale, and K. W. Lehnert, *Nature Physics* **4**, 929 (2008).
- [73] X. Zhou, V. Schmitt, P. Bertet, D. Vion, W. Wustmann, V. Shumeiko, and D. Esteve, *Phys. Rev. B* **89**, 214517 (2014).
- [74] C. Macklin, K. O'Brien, D. Hover, M. E. Schwartz, V. Bolkhovskiy, X. Zhang, W. D. Oliver, and I. Siddiqi, *Science* **350**, 307 (2015).
- [75] N. Bergeal, F. Schackert, M. Metcalfe, R. Vijay, V. E. Manucharyan, L. Frunzio, D. E. Prober, R. J. Schoelkopf, S. M. Girvin, and M. H. Devoret, *Nature* **465**, 64 (2010).
- [76] D. Marković, S. Jezouin, Q. Ficheux, S. Fedortchenko, S. Felicetti, T. Coudreau, P. Milman, Z. Leghtas, and B. Huard, *Phys. Rev. Lett.* **121**, 040505 (2018).
- [77] M. Foss-Feig, Z.-X. Gong, A. V. Gorshkov, and C. W. Clark, *arXiv preprint* (2016), 1612.07805.
- [78] M. A. Perlin, C. Qu, and A. M. Rey, *Phys. Rev. Lett.* **125**, 223401 (2020).
- [79] C. W. Gardiner and P. Zoller, *Quantum Noise* (Springer-Verlag, Berlin Heidelberg, 2000).
- [80] G. S. Agarwal, R. R. Puri, and R. P. Singh, *Phys. Rev. A* **56**, 2249 (1997).
- [81] R. Kubo, *Journal of the Physical Society of Japan* **17**, 1100 (1962).
- [82] M. Zens, D. O. Krimer, and S. Rotter, *Phys. Rev. A* **100**, 013856 (2019).
- [83] S. G. Schirmer and X. Wang, *Phys. Rev. A* **81**, 062306 (2010).
- [84] R. Grimm, M. Weidemüller, and Y. B. Ovchinnikov, *Advances in Atomic, Molecular and Optical Physics Advances In Atomic, Molecular, and Optical Physics*, **42**, 95 (2000).
- [85] D. M. Brink and G. R. Satchler, *Angular momentum* (Clarendon Press, Oxford, 1968).
- [86] F. Damanet, D. Braun, and J. Martin, *Phys. Rev. A* **94**, 033838 (2016).
- [87] N. Shammah, S. Ahmed, N. Lambert, S. De Liberato, and F. Nori, *Physical Review A* **98**, 063815 (2018).
- [88] D. Bacon, I. L. Chuang, and A. W. Harrow, *Phys. Rev. Lett.* **97**, 170502 (2006).
- [89] P. A. Vetter, L. Wang, D.-W. Wang, and M. O. Scully, *Physica Scripta* **91**, 023007 (2016).

## Appendix A: Adiabatic elimination of a cavity coupled to a squeezed bath

In this Appendix, we outline the derivation of the effective quantum master equation (11) of the main text. Our starting point is Eq. (9) describing a collection of spins interacting with a squeezed bosonic mode. For the moment, we ignore the terms in Eq. (9) describing local dissipation of the spins,

$$\begin{aligned} \frac{d}{dt}\hat{\rho} = & -ig\left[\hat{S}_+\hat{a} + \hat{S}_-\hat{a}^\dagger, \hat{\rho}\right] + \kappa_{\text{int}}\mathcal{D}[\hat{a}]\hat{\rho} \\ & + \kappa_{\text{sqz}}\mathcal{D}\left[\cosh(r)\hat{a} + \sinh(r)\hat{a}^\dagger\right]\hat{\rho}. \end{aligned} \quad (\text{A1})$$

Assuming that the cavity evolves on a much shorter timescale than the spins,

$$\kappa_{\text{int}} + \kappa_{\text{sqz}} \gg g\sqrt{N}, \quad (\text{A2})$$

we adiabatically eliminate the cavity by a projection operator technique [79] similar to the calculation outlined in Ref. 80. To this end, we split the quantum master equation into two superoperators,

$$\begin{aligned} \frac{d}{dt}\hat{\rho} &= \mathcal{L}_{\text{cav}}\hat{\rho} + \mathcal{L}_{\text{int}}\hat{\rho}, \quad (\text{A3}) \\ \mathcal{L}_{\text{cav}}\hat{\rho} &= \kappa_{\text{int}}\mathcal{D}[\hat{a}]\hat{\rho} + \kappa_{\text{sqz}}\mathcal{D}\left[\cosh(r)\hat{a} + \sinh(r)\hat{a}^\dagger\right]\hat{\rho}, \\ \mathcal{L}_{\text{int}}\hat{\rho} &= -ig\left[\hat{S}_+\hat{a} + \hat{S}_-\hat{a}^\dagger, \hat{\rho}\right], \end{aligned}$$

where  $\mathcal{L}_{\text{int}}\hat{\rho}$  is considered to be constant on the timescale defined by  $\mathcal{L}_{\text{cav}}\hat{\rho}$ . Using this approximation, we can formally solve Eq. (A3),

$$\hat{\rho}(t) = e^{\mathcal{L}_{\text{cav}}t}\hat{\rho}(0) + e^{\mathcal{L}_{\text{cav}}t}\int_0^t dt' e^{-\mathcal{L}_{\text{cav}}t'}\mathcal{L}_{\text{int}}\hat{\rho}(t'). \quad (\text{A4})$$

Performing a Born approximation, we decompose the state as  $\hat{\rho}(t) \approx \hat{\rho}_{\text{sp}}(t) \otimes \hat{\rho}_{\text{cav}}^{\text{ss}}$ , where  $\hat{\rho}_{\text{sp}}(t)$  is the reduced density matrix of the spin system and  $\hat{\rho}_{\text{cav}}^{\text{ss}}$  is the steady state of  $\mathcal{L}_{\text{cav}}$ . The equation of motion of the reduced spin density matrix is

$$\begin{aligned} \frac{d}{dt}\hat{\rho}_{\text{sp}}(t) &= \int_0^t dt' \text{Tr}_{\text{cav}}\left[\mathcal{L}_{\text{int}}e^{\mathcal{L}_{\text{cav}}(t-t')}\mathcal{L}_{\text{int}}\hat{\rho}_{\text{sp}}(t') \otimes \hat{\rho}_{\text{cav}}^{\text{ss}}\right]. \end{aligned} \quad (\text{A5})$$

Inserting the explicit form of  $\mathcal{L}_{\text{int}}$ , we find that the integral on the right-hand side of Eq. (A5) depends on the cavity correlation functions

$$\begin{aligned} & \text{Tr}_{\text{cav}}\left[\hat{a}^{(\dagger)}e^{\mathcal{L}_{\text{cav}}t}\hat{a}^{(\dagger)}\hat{\rho}_{\text{cav}}^{\text{ss}}\right] \\ &= \text{Tr}_{\text{cav}}\left[\hat{a}^{(\dagger)}e^{\mathcal{L}_{\text{cav}}t}\hat{\rho}_{\text{cav}}^{\text{ss}}\hat{a}^{(\dagger)}\right] \\ &= \frac{\kappa_{\text{sqz}}}{\kappa_{\text{sqz}} + \kappa_{\text{int}}}\sinh(r)\cosh(r)e^{-(\kappa_{\text{sqz}}+\kappa_{\text{int}})t/2}, \end{aligned} \quad (\text{A6})$$

$$\begin{aligned} \text{Tr}_{\text{cav}}\left[\hat{a}e^{\mathcal{L}_{\text{cav}}t}\hat{a}^\dagger\hat{\rho}_{\text{cav}}^{\text{ss}}\right] &= \text{Tr}_{\text{cav}}\left[\hat{a}^\dagger e^{\mathcal{L}_{\text{cav}}t}\hat{\rho}_{\text{cav}}^{\text{ss}}\hat{a}\right] \\ &= \frac{\kappa_{\text{sqz}}\cosh^2(r) + \kappa_{\text{int}}}{\kappa_{\text{sqz}} + \kappa_{\text{int}}}e^{-(\kappa_{\text{sqz}}+\kappa_{\text{int}})t/2}, \end{aligned} \quad (\text{A7})$$

$$\begin{aligned} \text{Tr}_{\text{cav}}\left[\hat{a}^\dagger e^{\mathcal{L}_{\text{cav}}t}\hat{a}\hat{\rho}_{\text{cav}}^{\text{ss}}\right] &= \text{Tr}_{\text{cav}}\left[\hat{a}e^{\mathcal{L}_{\text{cav}}t}\hat{\rho}_{\text{cav}}^{\text{ss}}\hat{a}^\dagger\right] \\ &= \frac{\kappa_{\text{sqz}}}{\kappa_{\text{sqz}} + \kappa_{\text{int}}}\sinh^2(r)e^{-(\kappa_{\text{sqz}}+\kappa_{\text{int}})t/2}. \end{aligned} \quad (\text{A8})$$

These correlation functions decay fast compared to the timescale on which  $\hat{\rho}_{\text{sp}}$  evolves, therefore, we can perform the Markov approximation  $\hat{\rho}_{\text{sp}}(t') \approx \hat{\rho}_{\text{sp}}(t)$  and rewrite Eq. (A5) as follows:

$$\begin{aligned} \frac{d}{dt}\hat{\rho}_{\text{sp}} &= \frac{4g^2}{(\kappa_{\text{sqz}} + \kappa_{\text{int}})^2}\left(\kappa_{\text{int}}\mathcal{D}\left[\hat{S}_-\right]\hat{\rho}_{\text{sp}}\right. \\ &\quad \left.+ \kappa_{\text{sqz}}\mathcal{D}\left[\cosh(r)\hat{S}_- - \sinh(r)\hat{S}_+\right]\hat{\rho}_{\text{sp}}\right). \end{aligned} \quad (\text{A9})$$

Taking into account the remaining terms in Eq. (9) describing single-spin dissipation, we recover Eq. (11) of the main text.

## Appendix B: Mean-field theory equations of motion

In this section, we provide the set of nonlinear equations of motion for the effective spin-only model considered in the main text, namely Eq. (11). While such a system of equations is not closed, we neglect third-order cumulants (equivalently performing a 2<sup>nd</sup>-order cumulant expansion) [81, 82], which lets us approximate the third-order expectation values of various operators as

$$\begin{aligned} \langle\hat{A}_i\hat{A}_j\hat{A}_k\rangle &\approx \langle\hat{A}_i\hat{A}_j\rangle\langle\hat{A}_k\rangle + \langle\hat{A}_i\hat{A}_k\rangle\langle\hat{A}_j\rangle \\ &\quad + \langle\hat{A}_j\hat{A}_k\rangle\langle\hat{A}_i\rangle - 2\langle\hat{A}_i\rangle\langle\hat{A}_j\rangle\langle\hat{A}_k\rangle. \end{aligned} \quad (\text{B1})$$

Hence, given the initial state with spins completely polarized along the  $-z$  direction (*i.e.*,  $\langle\hat{S}_z\rangle = -N/2$ ), the evolution is governed by the equations

$$\begin{aligned} \partial_t\langle\hat{S}_z\rangle &= \left(-\frac{e^{-2r}\Gamma}{2} - \frac{e^{2r}\Gamma}{2} - \gamma_{\text{coll}} - \gamma_{\text{rel}}\right)\langle\hat{S}_z\rangle \\ &\quad + (-\Gamma - \gamma_{\text{coll}})\left(\langle\hat{S}_x^2\rangle + \langle\hat{S}_y^2\rangle\right) - \frac{\gamma_{\text{rel}}N}{2}, \end{aligned} \quad (\text{B2})$$

$$\begin{aligned} \partial_t\langle\hat{S}_x^2\rangle &= (e^{2r}\Gamma + \gamma_{\text{coll}})\langle\hat{S}_z\rangle^2 \\ &\quad + \left((2\Gamma + 2\gamma_{\text{coll}})\langle\hat{S}_x^2\rangle - \frac{\Gamma}{2} - \frac{\gamma_{\text{coll}}}{2}\right)\langle\hat{S}_z\rangle \\ &\quad + (-e^{2r}\Gamma - \gamma_{\text{coll}} - 2\gamma_\phi - \gamma_{\text{rel}})\langle\hat{S}_x^2\rangle \\ &\quad + (e^{2r}\Gamma + \gamma_{\text{coll}})\langle\hat{C}_{ZZ}\rangle + \frac{N(\gamma_\phi + \frac{\gamma_{\text{rel}}}{2})}{2}, \end{aligned} \quad (\text{B3})$$

$$\begin{aligned}
\partial_t \langle \hat{S}_y^2 \rangle &= (e^{-2r} \Gamma + \gamma_{\text{coll}}) \langle \hat{S}_z \rangle^2 \\
&+ \left( (2\Gamma + 2\gamma_{\text{coll}}) \langle \hat{S}_y \rangle - \frac{\Gamma}{2} - \frac{\gamma_{\text{coll}}}{2} \right) \langle \hat{S}_z \rangle \\
&+ (-e^{-2r} \Gamma - \gamma_{\text{coll}} - 2\gamma_\phi - \gamma_{\text{rel}}) \langle \hat{S}_y^2 \rangle \\
&+ (e^{-2r} \Gamma + \gamma_{\text{coll}}) \langle \hat{C}_{ZZ} \rangle + \frac{N(\gamma_\phi + \frac{\gamma_{\text{rel}}}{2})}{2}, \quad (\text{B4})
\end{aligned}$$

$$\begin{aligned}
\partial_t \langle \hat{C}_{ZZ} \rangle &= (\gamma_{\text{coll}} + \Gamma + \gamma_{\text{rel}}) \langle \hat{S}_z \rangle + (e^{2r} \Gamma + \gamma_{\text{coll}}) \langle \hat{S}_x^2 \rangle \\
&+ (-e^{-2r} \Gamma - e^{2r} \Gamma - 2\gamma_{\text{coll}} - 2\gamma_{\text{rel}}) \langle \hat{C}_{ZZ} \rangle \\
&+ (e^{-2r} \Gamma + \gamma_{\text{coll}}) \langle \hat{S}_y^2 \rangle + \frac{\gamma_{\text{rel}} N}{2}, \quad (\text{B5})
\end{aligned}$$

where  $\langle \hat{C}_{ZZ} \rangle = \langle \hat{S}_z^2 \rangle - \langle \hat{S}_z \rangle \langle \hat{S}_z \rangle$ . We stress that if we assume that Eq. (11) is a result of coupling the spin system to a cavity interacting with an engineered squeezed reservoir with photon loss  $\kappa_{\text{int}}$ , then we have

$$\Gamma = \frac{4g^2}{(\kappa_{\text{sqz}} + \kappa_{\text{int}})^2} \kappa_{\text{sqz}}, \quad (\text{B6})$$

and

$$\gamma_{\text{coll}} = \frac{4g^2}{(\kappa_{\text{sqz}} + \kappa_{\text{int}})^2} \kappa_{\text{int}}, \quad (\text{B7})$$

as discussed in the main text and shown in detail in App. A.

### Appendix C: Cooperativity scaling of the $\xi_R^2$ parameter

In this Appendix, we provide a derivation of the cooperativity scaling of the Wineland parameter  $\xi_R^2$ . We concentrate our analysis on the weak dephasing limit, and start with the case where  $\gamma_\phi = 0$  and where only the local decay  $\gamma_{\text{rel}}$  as well as the collective cavity-induced decay  $\gamma_{\text{coll}}$  are present. A scenario where local spin dephasing is dominant can lead to substantially altered behavior of the system, and is the subject of Sec. V and App. E.

#### 1. Analytical derivation

We begin by linearizing the mean-field-theory equations of motion shown in App. B by focusing on the limit where  $\langle \hat{S}_z \rangle$  stays fixed at  $-N/2$ . This approximation closely reflects the true system dynamics when the spin number  $N$  is large and when the single cooperativities  $\eta_\phi$  or  $\eta_{\text{rel}}$  are not much larger than unity, resulting in effective spin squeezing that is far from the Heisenberg limit. Hence,

taking  $\langle \hat{S}_z \rangle = -N/2$  (*i.e.*, spins keeping their polarization throughout the evolution and in the steady state), the Wineland parameter takes a simple form,

$$\xi_R^2 = \frac{4}{N} \langle \hat{S}_y^2 \rangle_{\text{ss}}, \quad (\text{C1})$$

which we can write using the results in App. B as

$$\xi_R^2 = \frac{(N+1)\gamma_{\text{coll}} + (Ne^{-2r} + 1)\Gamma + \gamma_{\text{rel}}}{(N+1)\gamma_{\text{coll}} + (N + e^{-2r})\Gamma + \gamma_{\text{rel}}}. \quad (\text{C2})$$

Note that  $\xi_R^2$  gets smaller as  $r$  increases and hence, in what follows, we will take the limit  $r \rightarrow \infty$ . It is worth pointing out, however, that choosing a finite  $r$  which satisfies  $\exp(-2r) \ll 1/\sqrt{C_{\text{rel}}}$  is sufficient to reproduce the scaling of  $\xi_R^2$  derived below. In the large- $r$  limit, we find

$$\xi_R^2 = \frac{(N+1)\gamma_{\text{coll}} + \Gamma + \gamma_{\text{rel}}}{(N+1)\gamma_{\text{coll}} + \Gamma N + \gamma_{\text{rel}}}. \quad (\text{C3})$$

Next, we use Eqs. (12) and (13) of the main text to rewrite the above expression as

$$\xi_R^2 = \frac{\frac{N+1}{N}\kappa_{\text{int}} + \frac{(\kappa_{\text{sqz}} + \kappa_{\text{int}})^2}{4G^2}\gamma_{\text{rel}} + \frac{\kappa_{\text{sqz}}}{N}}{\frac{N+1}{N}\kappa_{\text{int}} + \frac{(\kappa_{\text{sqz}} + \kappa_{\text{int}})^2}{4G^2}\gamma_{\text{rel}} + \kappa_{\text{sqz}}}. \quad (\text{C4})$$

We consider a limit where  $N \rightarrow \infty$ , while  $G = \sqrt{N}g$  stays fixed. In such a case, the last term of the numerator can be dropped. Here it is crucial to point out that in an experimental setting, one will typically not have much control over  $\kappa_{\text{int}}$  and  $\gamma_{\text{rel}}$ , while  $\kappa_{\text{sqz}}$  can be tuned at will through appropriate reservoir engineering (see Sec. VI). Hence, it is important to understand what value of  $\kappa_{\text{sqz}}$  should be chosen to maximize the amount squeezing that this protocol can achieve. At first glance, one might think that choosing  $\kappa_{\text{sqz}}$  as large as possible (*i.e.*,  $\kappa_{\text{sqz}} \rightarrow \infty$ ) is ideal as that maximizes the amount of bosonic squeezing that the spin-coupled cavity experiences. From Eq. (12), however, we see that such a choice will actually limit the value of  $\Gamma$ , which directly impacts the strength of squeezed-vacuum reservoir that the spins see [see Eq. (11) in the main text], resulting in the squeezing performance being strongly limited by the value of  $\gamma_{\text{rel}}$ . Hence, as we shall see shortly, the right thing to do is to still choose  $\kappa_{\text{sqz}} \gg \kappa_{\text{int}}, \gamma_{\text{rel}}$ , but yet not too large, so that the  $\Gamma$ -controlled process is dominant over the local spin decay  $\gamma_{\text{rel}}$ . To see this explicitly, we minimize Eq. (C4) with respect to  $\kappa_{\text{sqz}}$ . Assuming  $N \gg 1$ , this leads to

$$\begin{aligned}
\xi_R^2 &\approx 2 \left( \sqrt{\frac{4G^2}{\kappa_{\text{int}}\gamma_{\text{rel}}} + 1} + 1 \right)^{-1} \\
&= \frac{2}{\sqrt{C_{\text{rel}}}} + \mathcal{O}\left(\frac{1}{C_{\text{rel}}}\right), \quad (\text{C5})
\end{aligned}$$

where, in the second line, we used Eq. (10) of the main text to express the result in terms of the collective cooperativity  $\mathcal{C}_{\text{rel}}$  and then expanded in the limit of large  $\mathcal{C}_{\text{rel}}$ . Our above expression shows the  $\mathcal{C}_{\text{rel}}^{-1/2}$  cooperativity scaling for the dissipative protocol, which outperforms the  $\mathcal{C}_{\text{rel}}^{-1/3}$  behavior of the OAT method [35], in the case where spin decay is the dominant local noise process. The optimal value of  $\kappa_{\text{sqz}}$  that results in Eq. (C5) reads

$$\begin{aligned} \kappa_{\text{sqz}}^{\text{opt}} &= \left( \kappa_{\text{int}}^2 + \frac{4G^2 \kappa_{\text{int}}}{\gamma_{\text{rel}}} \right)^{\frac{1}{2}} \\ &\approx 2G \sqrt{\frac{\kappa_{\text{int}}}{\gamma_{\text{rel}}}} = \kappa_{\text{int}} \sqrt{\mathcal{C}_{\text{rel}}}, \end{aligned} \quad (\text{C6})$$

which confirms the need for  $\kappa_{\text{sqz}} \gg \kappa_{\text{int}}$  (given large  $\mathcal{C}_{\text{rel}}$ ), while also showing that it should not be infinitely large. Finally, we stress that  $\xi_R^2$  is ultimately limited by  $\kappa_{\text{int}}/(\kappa_{\text{int}} + \kappa_{\text{sqz}})$ , hence it is crucial that an appropriate  $\kappa_{\text{sqz}}$  can be realized in an experimental setting.

While the above result has been calculated in the limit where  $\gamma_\phi = 0$ , a similar expression is valid when some local dephasing is present (*i.e.*,  $\gamma_\phi \neq 0$ ). In such a case, one can simply assume  $\gamma_{\text{rel}} \rightarrow \gamma_{\text{rel}} + 2\gamma_\phi$  in Eq. (C4). As discussed in more detail in Sec. V of the main text, however, this is only true when  $\gamma_\phi$  is not too large, namely when  $\gamma_\phi \lesssim N\gamma_{\text{rel}}$ . Otherwise, a local dephasing process can have a significant impact on the evolution and therefore dramatically limit the steady state performance of the protocol.

## 2. Mean-field theory simulations

In this section, we present mean-field-theory simulations of the dissipative protocol obtained using the full (nonlinear) equations shown in App. B. We consider the case where local spin decay dominates over local spin dephasing, and in particular work in the limit of  $\gamma_\phi = 0$ .

The plot in Fig. S1, shows the scaling of the Wineland parameter as a function of the collective cooperativity  $\mathcal{C}_{\text{rel}}$ . The parameters are  $\kappa_{\text{int}} = 500g$ ,  $\gamma_{\text{rel}} = 0.04g$ , giving  $\eta_{\text{rel}} = 0.2$ , while the number  $N$  of spins is varied in order to modify  $\mathcal{C}_{\text{rel}}$ . At each blue point, both  $r$  and  $\kappa_{\text{sqz}}$  are optimized in order to minimize  $\xi_R^2$ . The orange curve shows the corresponding fit, which is calculated using the three data points with largest  $\mathcal{C}_{\text{rel}}$ . We see good agreement with the cooperativity scaling discussed in the main text and derived in detail in the section above (where we have linearized the equations of motion). For comparison, the black dashed line describes the optimized squeezing of the engineered bosonic reservoir. The black solid line shows an ideal Heisenberg

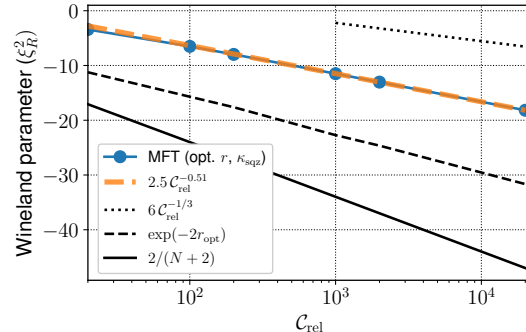


FIG. S1. Scaling of the Wineland parameter  $\xi_R^2$  as a function of collective cooperativity  $\mathcal{C}_{\text{rel}}$ . The blue curve corresponds to  $\xi_R^2$  calculated by evolving the full (non-linear) mean-field equations of motion for the dissipative system (see App. B). Here  $\kappa_{\text{int}} = 500g$ ,  $\gamma_{\text{rel}} = 0.04g$ , giving  $\eta_{\text{rel}} = 0.2$ . The number  $N$  of spins is changed in order to vary  $\mathcal{C}_{\text{rel}}$ . At each blue point, both  $r$  and  $\kappa_{\text{sqz}}$  are optimized in order to minimize  $\xi_R^2$ . The orange dashed curve shows the corresponding fit (calculated over the three data points with the largest  $\mathcal{C}_{\text{rel}}$ ). The black dashed line describes the optimized squeezing of the engineered bosonic reservoir. The solid black line shows an ideal Heisenberg scaling  $2/(N+2)$ . Finally, the black dotted curve shows the OAT scaling as calculated in [35].

scaling  $2/(N+2)$ . We also plot the dotted black curve, which corresponds to the squeezing one would get from the OAT protocol in the limit where  $\gamma_{\text{rel}}$  dominates over  $\gamma_\phi$  (in the large  $\mathcal{C}_{\text{rel}}$  limit) – see Ref. [35]. The simulations confirm that the dissipative protocol can indeed outperform the OAT approach.

## Appendix D: Even-odd effect

In this Appendix, we briefly review previous results on the dissipative steady state of Eq. (2) in the main text and we derive Eq. (16) of the main text. We then comment on variance detection measurements required to use the even-odd effect as a sensor, and we discuss the impact of local dissipation.

### 1. Properties of the steady state

Agarwal and Puri derived that the steady state of Eq. (2) is

$$\hat{\rho}_{\text{ss}}^{(j)} \propto \hat{\Sigma}^{-1} (\hat{\Sigma}^\dagger)^{-1} = (\hat{\Sigma}^\dagger \hat{\Sigma})^{-1}, \quad (\text{D1})$$

if the Hermitian operator  $\hat{\Sigma}^\dagger \hat{\Sigma}$  is invertible [22]. Using the non-unitary transformation  $e^{\theta \hat{S}_z}$ , where



$\theta(r) = \ln \sqrt{\tanh(r)}$ , one can express the jump operator  $\hat{\Sigma}(r)$  as

$$\hat{\Sigma}(r) = -2i \sqrt{\sinh(r) \cosh(r)} e^{\theta(r) \hat{S}_z} \hat{S}_y e^{-\theta(r) \hat{S}_z}. \quad (\text{D2})$$

Therefore, the eigenstates of  $\hat{\Sigma}(r)$  are

$$|j, m(r)\rangle \propto e^{\theta(r) \hat{S}_z} |j, m\rangle_y, \quad (\text{D3})$$

where  $|j, m\rangle_y$  are the eigenstates of  $\hat{S}_y$  corresponding to an eigenvalue  $m \in \{-j, \dots, j\}$  [22].

If  $N$  is odd, both  $\hat{\Sigma}(r)$  and  $\hat{\Sigma}^\dagger(r)$  have only nonzero eigenvalues and  $\hat{\Sigma}(r)^\dagger \hat{\Sigma}(r)$  is invertible. Defining the eigenstates of  $\hat{\Sigma}(r)^\dagger \hat{\Sigma}(r)$ ,

$$\hat{\Sigma}(r)^\dagger \hat{\Sigma}(r) |\psi_k\rangle = \lambda_k |\psi_k\rangle, \quad (\text{D4})$$

with positive eigenvalues  $0 < \lambda_0 \leq \dots \leq \lambda_{2j}$ , one can evaluate Eq. (D1) and obtains

$$\hat{\rho}_{\text{ss}}^{(j)} = \frac{1}{\sum_{k=0}^{2j} \frac{1}{\lambda_k}} \sum_{k=0}^{2j} \frac{1}{\lambda_k} |\psi_k\rangle \langle \psi_k|, \quad (\text{D5})$$

which is expression (16) of the main text. This is the generic form for the steady state of a master equation with a single jump operator that has no zero eigenvalues [83].

If  $N$  is even,  $\hat{\Sigma}(r)$  has a zero eigenvalue in each subspace of angular momentum  $j$  and the associated eigenstates are the dark states

$$|\psi_{\text{dk}}[j; r]\rangle \propto e^{\theta(r) \hat{S}_z} |j, 0\rangle_y, \quad (\text{D6})$$

given by Eq. (6) of the main text. These dark states are zero eigenstates of  $\hat{\Sigma}(r)^\dagger \hat{\Sigma}(r)$  too, therefore,  $\hat{\Sigma}(r)^\dagger \hat{\Sigma}(r)$  is not invertible. Informally speaking, if one inverted  $\hat{\Sigma}(r)^\dagger \hat{\Sigma}(r)$  in the presence of a zero eigenvalue, the term in Eq. (D5) associated with the zero eigenvalue would diverge and only the dark state would contribute to  $\hat{\rho}_{\text{ss}}^{(j)}$  after normalization,  $\hat{\rho}_{\text{ss}}^{(j)}(r) = |\psi_{\text{dk}}[j; r]\rangle \langle \psi_{\text{dk}}[j; r]|$ .

## 2. Using the even-odd effect for sensing

As described in Sec. III D of the main text, the sensitivity of the steady state on the parity of the number  $N$  of spins can be used for sensing. Experimentally, sudden changes in the parity of  $N$  can be induced by various mechanisms. Trapped atoms can be physically lost from the trap by collisions with background gas, internal collisions, and photon-assisted processes [84]. If the spin-1/2 degree of freedom is a subspace of an atomic multi-level

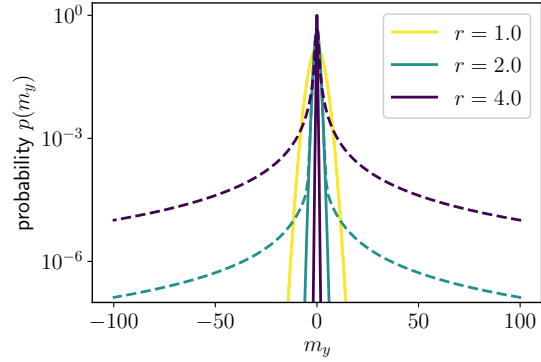


FIG. S2.  $\hat{S}_y$  probability distribution of the steady state of Eq. (2) for  $N = 200$  (solid lines) vs.  $N = 201$  (dashed lines). The probability distributions for even and odd  $N$  differ if the relation  $e^{2r} \gtrsim N$  holds. In the limit  $e^{2r} \gg N$ , the odd- $N$  distribution develops a fat tail of large fluctuations.

structure, undesired internal transitions can occur, which take the atom out of the spin-1/2 subspace and effectively remove it from the collective dynamics even though it may still be trapped [25]. Moreover, one could devise a system where the coupling strength of a single spin to the cavity and, thus, to the collective spin depends on an external parameter. A change of this single-spin coupling strength modifies the number of collective spins, which is collectively amplified and yields a large change of the steady state.

Note that such effective atom loss events do not change the collective expectation value  $\langle \hat{S}_y \rangle = 0$  of the distribution. However, the statistics of the fluctuations  $\langle \hat{S}_y^2 \rangle$  depends on the parity, as shown in Fig. S2. The parity of  $N$  can thus be inferred by imposing a threshold condition on the variance  $\langle \hat{S}_y^2 \rangle$  measured using spin-noise spectroscopy [51–56].

## 3. Impact of local dissipation

So far, our analysis of even-odd effects in the steady state has focused on the idealized case without any single-spin dissipation:  $\gamma_{\text{rel}} = \gamma_\phi = \gamma_{\text{coll}} = 0$ . We found that the Wineland parameters for even and odd  $N$  differ strongly in the regime  $r \gg r_{\text{crit}}$ , as shown in Fig. 3 of the main text. Figure S3 shows that if local dissipation is taken into account, spin squeezing is reduced but the ratio between the Wineland parameters for even and odd  $N$  remains large. Moreover, for a fixed value of the squeezing parameter  $r$ , the ratio of the Wineland parameters in the presence of local dephasing can even be larger than the corresponding ratio obtained for  $\gamma_\phi = 0$ .

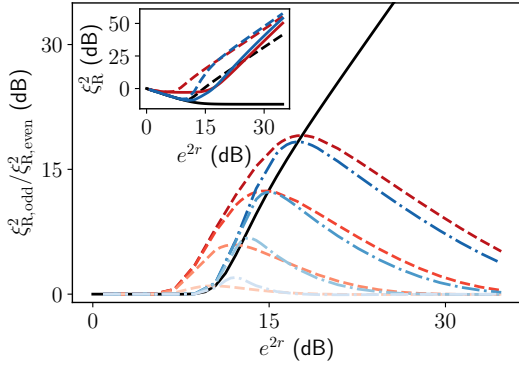


FIG. S3. Ratio between the steady-state Wineland parameters for even and odd  $N$  without local dissipation (solid black line), with local dephasing (dashed lines), and with local relaxation (dash-dotted lines), calculated using the quantum master equation Eq. (11) of the main text. The parameters are from top to bottom:  $\gamma_\phi/\Gamma = (0.00005, 0.0005, 0.005, 0.05)$  and  $\gamma_{\text{rel}}/\Gamma = 0$  for the red curves and  $\gamma_{\text{rel}}/\Gamma = (0.0001, 0.001, 0.01, 0.1)$  and  $\gamma_\phi/\Gamma = 0$  for the blue curves. **Inset:** Corresponding plot of the Wineland parameters for  $N = 30$  (solid lines) vs.  $N = 31$  (dashed lines) without local dissipation (black lines), with local dephasing (red lines,  $\gamma_\phi/\Gamma = 0.00005$ ,  $\gamma_{\text{rel}}/\Gamma = 0$ ), and with local relaxation (blue lines,  $\gamma_\phi/\Gamma = 0$ ,  $\gamma_{\text{rel}}/\Gamma = 0.0001$ ).

For fixed local dissipation rates, the ratio is largest around the onset of the even-odd effect,  $r_{\text{max}} \approx r_{\text{crit}}$ . At this optimum squeezing parameter  $r_{\text{max}}$ , effective single-spin cooperativities much larger than unity,  $\Gamma/\gamma_\phi \gg 1$  or  $\Gamma/\gamma_{\text{rel}} \gg 1$ , are required to observe a ratio of the Wineland parameters greater than two.

### Appendix E: Liouvillian perturbation theory of the slow timescale

In this Appendix, we use Liouvillian perturbation theory [57] to analyze the emergence of the long relaxation timescale in the presence of local dephasing, which has been discussed in Sec. V of the main text. We also provide a simple physical argument to understand this effect.

#### 1. Hilbert space of $N$ spin-1/2 systems and permutational invariance

Addition of angular momenta of  $N$  spin-1/2 systems gives rise to  $\lfloor N/2 \rfloor + 1$  subspaces of total angular momentum  $j$ , where  $j$  takes values between  $j_{\text{max}} = N/2$  and  $j_{\text{min}} = 0$  (1/2) if  $N$  is even (odd) [85]. For  $N > 2$ , all but the maximum-angular-

momentum subspace are degenerate since there are multiple ways to combine  $N$  spin 1/2 systems to a total angular momentum  $j < N/2$  [33] (for an illustration, see, *e.g.*, Ref. 86). If local dissipative processes act *identically* on each spin-1/2 system, the equations of motion are invariant under permutation of the spins [34]. Consequently, if the system is initialized in a permutationally invariant state, *e.g.*, any state in the subspace  $j = j_{\text{max}}$ , the collective and local dissipative processes will preserve the permutational symmetry. Exploiting this symmetry, one can derive an effective quantum master equation which requires significantly less degrees of freedom to describe the system [34] and gives rise to efficient numerical simulation of large spin ensembles [87].

#### 2. Analysis of the slow timescale

Our starting point, the quantum master equation (11) of the main text, belongs to the class of permutationally invariant systems described above. In the following, we focus on the case  $\gamma_{\text{coll}} = \gamma_{\text{rel}} = 0$ . Introducing the dimensionless time  $\tau = \Gamma t$ , the equation can be rewritten in the form  $d\hat{\rho}/d\tau = \mathcal{L}_0\hat{\rho} + \varepsilon\mathcal{L}_1\hat{\rho}$ , where we introduced the dimensionless superoperators

$$\mathcal{L}_0 = \mathcal{D} \left[ \hat{\Sigma}(r) \right], \quad (\text{E1})$$

$$\mathcal{L}_1 = \sum_{k=1}^N \mathcal{D} \left[ \frac{\hat{\sigma}_z^{(k)}}{2} \right], \quad (\text{E2})$$

and the dimensionless perturbation strength  $\varepsilon = 2\gamma_\phi/\Gamma$ . In the absence of local dephasing,  $\varepsilon = 0$ , the superoperator  $\mathcal{L}_0$  has  $\lfloor N/2 \rfloor + 1$  different steady states  $\hat{\rho}_0^{(j)}$ , each of them living in a different subspace of collective angular momentum  $j$ . Weak local dephasing,  $\gamma_\phi \ll \Gamma$ , enables incoherent transitions between adjacent angular-momentum subspaces [34]. This perturbation lifts the degeneracy of the steady states and opens a new dissipative gap that determines the relaxation timescale towards the new, unique steady state.

The first-order corrections to the vanishing eigenvalues of  $\mathcal{L}_0$  are given by the eigenvalues of the tridiagonal matrix

$$M_{j,j'} = \text{Tr} \left[ \hat{\mathbf{1}}^{(j')} \mathcal{L}_1 \hat{\rho}_0^{(j)} \right] \quad (\text{E3})$$

containing the transition rates  $j \rightarrow j'$  between collective angular momentum subspaces. Here,  $\hat{\mathbf{1}}^{(j)}$  is the identity operator in the angular-momentum subspace  $j$ . For even  $N$ , the transition rates are shown

in Fig. S4(a). They depend on the structure of the dark state (6) given in the main text,

$$\Gamma_{j \rightarrow j-1} = \sum_{m=-j+1}^{j-1} \Gamma_{j;m,m}^{(5)} |c_m^{(j)}|^2, \quad (\text{E4})$$

$$\Gamma_{j \rightarrow j+1} = \sum_{m=-j}^j \Gamma_{j;m,m}^{(6)} |c_m^{(j)}|^2, \quad (\text{E5})$$

where  $c_m^{(j)}$  are the expansion coefficients of the dark state and  $\Gamma_{j;m,m}^{(5,6)}$  are the transition rates derived in Ref. 34 using the notation introduced in Ref. 87. Note that, in our case,  $\mathcal{L}_1$  is dimensionless such that the transition rates (E4) and (E5) are dimensionless, too. The asymptotic decay rate, *i.e.*, the absolute value of the smallest gap in the spectrum of  $M$ , is shown in Fig. S4(b).

For  $r = 0$ , the unperturbed steady states are the ground states of each angular-momentum subspace,  $\hat{\rho}_0^{(j)} = |j, -j\rangle \langle j, -j|$ . Therefore, transitions are only possible towards subspaces of larger angular momentum,  $\Gamma_{j \rightarrow j-1} = 0$ , and the relaxation dynamics is dominated by the bottleneck of the smallest nonzero transition rate,  $\Gamma_{N/2-1, -N/2+1 \rightarrow N/2, -N/2+1} = 1/N$ .

For  $r \neq 0$ , transition rates  $\Gamma_{j \rightarrow j-1}$  are nonzero and dominate over the rate  $\Gamma_{N/2-1 \rightarrow N/2}$  if the condition  $r > 1/\sqrt{N}$  holds. As a consequence, an initial state in the maximum-angular-momentum subspace  $j = N/2$  will undergo a directed hopping process towards lower angular momentum subspaces until it reaches a subspace  $j_0$  where “downward” and “upward” rates are balanced,  $\Gamma_{j_0 \rightarrow j_0-1} \approx \Gamma_{j_0-1 \rightarrow j_0}$ . Note that the downward rates  $\Gamma_{j \rightarrow j-1}$  are almost constant as a function of  $j$  whereas the upward rates  $\Gamma_{j \rightarrow j+1}$  depend strongly on  $j$ , as shown in Fig. S4(a). The asymptotic decay rate towards the steady state is proportional to  $1/N$  if the transition rates in the vicinity of the equilibrium point  $j_0$  scale proportional to  $1/N$ . Inspection of the rates  $\Gamma_{j;m,m}^{(5,6)}$  listed in Ref. 87 shows that this is the case if  $j \gg N/2$  and  $m \ll 0$ . For a given squeezing parameter  $r$ , these conditions can be fulfilled if  $N$  is sufficiently large,

$$N \gg e^{ar}, \quad (\text{E6})$$

as shown in Fig. S4(b). Numerically, we find an exponent  $a \approx 5$ , see inset of Fig. S4(b).

In the limit  $r \rightarrow \infty$ , the asymptotic decay rate converges to the constant value  $1/2$ .

### 3. Physical argument for the slow timescale

The existence of a bottleneck relaxation rate causing a  $1/N$  scaling of the asymptotic decay rate for

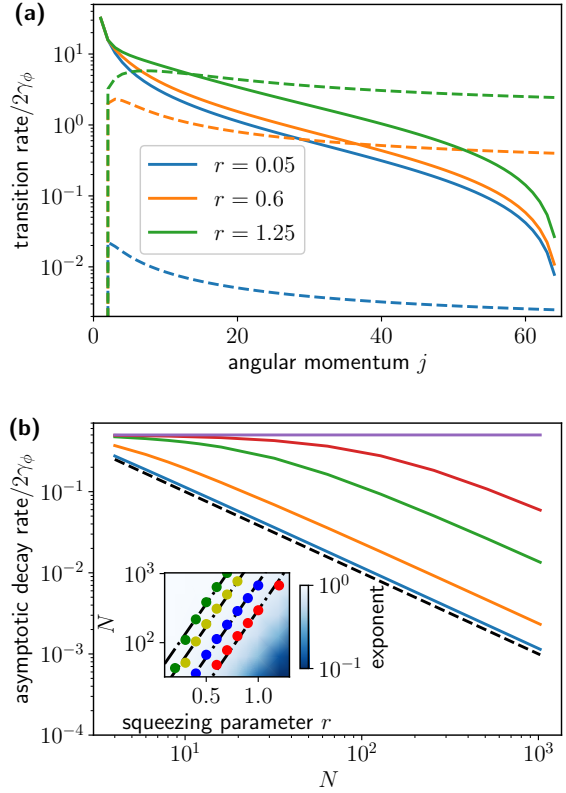


FIG. S4. (a) Transition rates  $j - 1 \rightarrow j$  (solid) and  $j \rightarrow j - 1$  (dashed) between different angular momentum subspaces due to local dephasing for  $N = 128$  and  $\Gamma = 1$ . (b) Asymptotic decay rate in the presence of local dephasing for  $r = 0.2, 0.5, 1.0, 1.4$ , and  $4.0$  (bottom to top). The dashed black line indicates  $1/N$  scaling obtained for  $r = 0$ . Inset Scaling exponent  $a$  in  $1/N^a$  as a function of  $N$  and  $r$ . The data points indicate the positions where  $a$  becomes smaller than 0.99, 0.98, 0.95, and 0.9 (left to right). The dash-dotted black lines are a guide to the eye and indicate  $e^{5r}$  scaling.

local dephasing can be understood by an intuitive argument. To explain it, we focus on the transition rate  $\Gamma_{N/2-1, -N/2+1 \rightarrow N/2, -N/2+1}$ , which is the bottleneck determining the asymptotic decay rate in the limit  $r < 1/\sqrt{N}$ . The states that are involved in this transition can be parametrized as [88, 89]

$$|p\rangle = \frac{1}{\sqrt{N}} \sum_{j=1}^N e^{2\pi i j p / N} |j\rangle, \quad (\text{E7})$$

where  $p \in \{0, \dots, N-1\}$ . Here,  $|j\rangle$  denotes the  $N$ -particle state where the  $j$ th spin is in the excited state and all others are in the ground state. The  $p = 0$  state has total angular momentum  $j = N/2$ ,

*i.e.*, we can identify it with the state

$$|\overline{0}\rangle \equiv |N/2, -N/2 + 1\rangle \quad (\text{E8})$$

in the maximum-angular-momentum subspace. In contrast, the  $N - 1$  states with  $p > 0$  have total angular momentum  $j = N/2 - 1$ . Therefore, the index  $p > 0$  allows us to label the  $N - 1$  degenerate states in the  $j = N/2 - 1$  subspace,

$$|\overline{p}\rangle \equiv |N/2 - 1, -N/2 + 1, p\rangle \text{ for } p > 0. \quad (\text{E9})$$

Local dephasing of spin  $n$  changes one sign in the superposition (E7),

$$\frac{1}{2}\hat{\sigma}_z^{(n)}|\overline{p}\rangle = -\frac{1}{2}|\overline{p}\rangle + \frac{1}{\sqrt{N}}e^{2\pi inp/N}|n\rangle, \quad (\text{E10})$$

and thus creates an overlap between the orthogonal states  $|\overline{0}\rangle$  and  $|\overline{p > 0}\rangle$  that is proportional to  $1/N$ ,

$$V_{0,p} = \langle \overline{0} | \frac{1}{2}\hat{\sigma}_z^{(n)} | \overline{p > 0} \rangle = \frac{1}{N}e^{2\pi inp/N}. \quad (\text{E11})$$

For identical dephasing processes on all  $N$  spins and for a collective initial state, *i.e.*, a uniform statistical mixture of all  $N - 1$  states  $|N/2 - 1, -N/2 + 1, p\rangle$ , the total upward transition rate between the two collective angular momentum subspaces is

$$\begin{aligned} & \Gamma_{N/2-1, -N/2+1 \rightarrow N/2, -N/2+1} \\ &= \sum_{p=1}^{N-1} \frac{1}{N-1} \sum_{n=1}^N |V_{0,p}|^2 = \frac{1}{N}, \end{aligned} \quad (\text{E12})$$

which is the bottleneck of the relaxation process and features the  $1/N$  scaling with system size. Note that the corresponding downward rate is of the order of unity because we have to sum over all  $N - 1$  possible target states  $|\overline{p > 0}\rangle$ , too,

$$\begin{aligned} & \Gamma_{N/2, -N/2+1 \rightarrow N/2-1, -N/2+1} \\ &= \sum_{p=1}^{N-1} \sum_{n=1}^N |V_{0,p}|^2 = \frac{N-1}{N}. \end{aligned} \quad (\text{E13})$$

Also note that local relaxation does *not* lead to a similar emergence of the slow timescale because the overlap corresponding to Eq. (E11) will only be proportional to  $1/\sqrt{N}$  and is thus canceled by the summation performed in Eq. (E12).

### Appendix F: Optimal parameters in master equations

In this section, we show how the optimal protocol parameters vary as a function of increasing system

size  $N$  in simulations from Fig. 5 of the main text. In the case of the dissipative protocols, the optimization included varying both  $r$  as well as  $\kappa_{\text{sqz}}$ , whereas in the case of OAT, the spins-cavity detuning  $\Delta_c$  (see App. G) is varied. The results are shown in Fig. S5

### Appendix G: Effective One-Axis Twist master equation

In this Appendix, we present the effective model that we consider when discussing the OAT protocol both in the main text and in App. C2. In particular, following [27, 35], we envision an ensemble of spins dispersively coupled to a bosonic cavity. After adiabatically eliminating the cavity, the spin-only master equation can be approximated by [35]

$$\begin{aligned} \dot{\hat{\rho}} = & -i\left[\chi\left(\hat{S}^2 - \hat{S}_z^2\right), \hat{\rho}\right] + \frac{\kappa_{\text{int}}g^2}{\Delta_c^2 + \left(\frac{\kappa_{\text{int}}}{2}\right)^2} \mathcal{D}\left[\hat{S}_-\right] \hat{\rho} \\ & + \gamma_{\text{rel}} \sum_k \mathcal{D}\left[\hat{\sigma}_-^{(k)}\right] \hat{\rho}, \end{aligned} \quad (\text{G1})$$

with

$$\chi = \frac{g^2\Delta_c}{\Delta_c^2 + \left(\frac{\kappa_{\text{int}}}{2}\right)^2}, \quad (\text{G2})$$

and with  $\Delta_c$  representing the cavity-spin detuning,  $g$  the cavity-spin coupling strength,  $\kappa_{\text{int}}$  the decay rate of the cavity, and  $\gamma_{\text{rel}}$  the local spin decay. We point out that we assume in the simulations that  $\Delta_c$  is a tunable parameter, over which we optimize in order to maximize the amount of spin squeezing that the protocol can achieve.

### Appendix H: Scaling of the Wineland parameter $\xi_R^2$ in the limit $\eta_{\text{rel}} \rightarrow \infty$

When analyzing the performance of the dissipative spin squeezing protocol in the main text, as one means of implementation, we envisioned engineering the required dissipator by coupling a spin ensemble to a lossy cavity that in turn interacts with an appropriately engineered squeezed bath. Furthermore, in our cooperativity scaling analysis (see Sec. IV and App. C) we investigated the limit of weak single spin cooperativity  $\eta_{\text{rel}} \leq 1$ . It is also interesting to consider a different asymptotic regime, where the internal cavity loss  $\kappa_{\text{int}}$  is negligible, giving an extremely large  $\eta_{\text{rel}}$ . We focus on the specific case where  $\kappa_{\text{int}} = 0$ , and the only undesired dynamics is due to single-spin relaxation at a rate  $\gamma_{\text{rel}}$ . Such a situation could be realized with any cavity, by

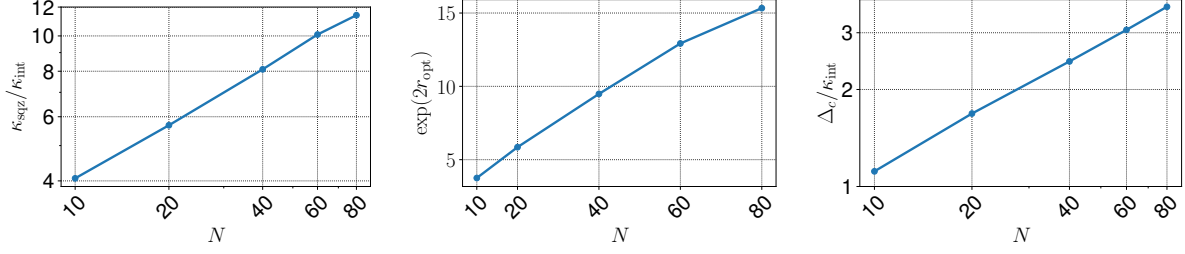


FIG. S5. Values of optimal parameters obtained from master equation simulations of both the dissipative as well as the OAT protocol, which were used to generate Fig. 5 of the main text. Left and center panels show the optimal values of  $\kappa_{\text{int}}$  and  $r$  (plot shows  $\exp(2r)$ ) that resulted from the dissipative protocol simulations. The right panel shows the optimal spin-cavity detuning that was used in for the OAT protocol. See Fig. 5 for details about the rest of the parameters that were used.

directly irradiating an ensemble of two-level atoms with squeezed light. While this situation was analyzed in Refs. [22, 24] the impacts of single spin relaxation were not studied.

The master equation in our chosen limit is thus

$$\dot{\rho} = \Gamma \mathcal{D} [\hat{\Sigma}[r]] \hat{\rho} + \gamma_{\text{rel}} \sum_k \mathcal{D} [\hat{\sigma}_-^{(k)}] \hat{\rho}. \quad (\text{H1})$$

The key dimensionless parameter that describes the competition of the desired collective dissipative dynamics and the unwanted relaxation is

$$\tilde{\eta} = \frac{\Gamma}{\gamma_{\text{rel}}}. \quad (\text{H2})$$

Once again concentrating our attention on the large- $N$  limit and fixing  $\langle \hat{S}_z \rangle = -N/2$ , we can approximate the Wineland parameter using the mean-field equations of App. B as

$$\xi_R^2 \approx \frac{\tilde{\eta} + 1}{N\tilde{\eta} + 1}. \quad (\text{H3})$$

In the above expression we have already taken the limit  $r \rightarrow \infty$ , which minimizes  $\xi_R^2$ . As one would expect, achievable squeezing increases as  $\tilde{\eta}$  gets larger, but more importantly we have that  $\xi_R^2 \propto 1/N$ . We can also define a quantity analogous to a collective cooperativity in this simplified system,

$$\tilde{\mathcal{C}} = N\tilde{\eta}, \quad (\text{H4})$$

which then lets us write

$$\xi_R^2 \propto \frac{1}{\tilde{\mathcal{C}}}, \quad (\text{H5})$$

assuming  $\tilde{\eta} \leq 1$  and  $\tilde{\mathcal{C}} \gg 1$ .

- 
- [1] M. Kitagawa and M. Ueda, *Phys. Rev. A* **47**, 5138 (1993).
  - [2] L. Pezzè, A. Smerzi, M. K. Oberthaler, R. Schmied, and P. Treutlein, *Rev. Mod. Phys.* **90**, 035005 (2018).
  - [3] I. D. Leroux, M. H. Schleier-Smith, and V. Vuletić, *Phys. Rev. Lett.* **104**, 073602 (2010).
  - [4] M. F. Riedel, P. Böhi, Y. Li, T. W. Hänsch, A. Sinatra, and P. Treutlein, *Nature* **464**, 1170 (2010).
  - [5] C. Gross, T. Zibold, E. Nicklas, J. Estève, and M. K. Oberthaler, *Nature* **464**, 1165 (2010).
  - [6] O. Hosten, R. Krishnakumar, N. J. Engelsens, and M. A. Kasevich, *Science* **352**, 1552 (2016).
  - [7] P. Cappellaro and M. D. Lukin, *Phys. Rev. A* **80**, 032311 (2009).
  - [8] Y. C. Liu, Z. F. Xu, G. R. Jin, and L. You, *Phys. Rev. Lett.* **107**, 013601 (2011).
  - [9] J. Borregaard, E. Davis, G. S. Bentsen, M. H. Schleier-Smith, and A. S. Sørensen, *New J. Phys.* **19**, 093021 (2017).
  - [10] P. Groszkowski, H.-K. Lau, C. Leroux, L. Govia, and A. Clerk, *Physical Review Letters* **125**, 203601 (2020).
  - [11] J. F. Poyatos, J. I. Cirac, and P. Zoller, *Phys. Rev. Lett.* **77**, 4728 (1996).
  - [12] J. I. Cirac, A. S. Parkins, R. Blatt, and P. Zoller, *Physical Review Letters* **70**, 556 (1993).
  - [13] A. Kronwald, F. Marquardt, and A. A. Clerk, *Phys.*

- Rev. A* **88**, 063833 (2013).
- [14] N. Didier, F. Qassemi, and A. Blais, *Physical Review A* **89**, 013820 (2014).
- [15] E. E. Wollman, C. U. Lei, A. J. Weinstein, J. Suh, A. Kronwald, F. Marquardt, A. A. Clerk, and K. C. Schwab, *Science* **349**, 952 (2015).
- [16] D. Kienzler, H.-Y. Lo, B. Keitch, L. d. Clercq, F. Leupold, F. Lindenfesler, M. Marinelli, V. Negnevitsky, and J. P. Home, *Science* **347**, 53 (2015).
- [17] F. Lecocq, J. B. Clark, R. W. Simmonds, J. Aumentado, and J. D. Teufel, *Phys. Rev. X* **5**, 041037 (2015).
- [18] J.-M. Pirkkalainen, E. Damskäg, M. Brandt, F. Massel, and M. A. Sillanpää, *Phys. Rev. Lett.* **115**, 243601 (2015).
- [19] C. U. Lei, A. J. Weinstein, J. Suh, E. E. Wollman, A. Kronwald, F. Marquardt, A. A. Clerk, and K. C. Schwab, *Phys. Rev. Lett.* **117**, 100801 (2016).
- [20] R. Dassonneville, R. Assouly, T. Peronnin, A. A. Clerk, A. Bienfait, and B. Huard, *arXiv preprint* (2021), 2102.02863v1.
- [21] G. S. Agarwal and R. R. Puri, *Optics Communications* **69**, 267 (1989).
- [22] G. S. Agarwal and R. R. Puri, *Phys. Rev. A* **41**, 3782 (1990).
- [23] G. S. Agarwal and R. R. Puri, *Phys. Rev. A* **49**, 4968 (1994).
- [24] A. Kuzmich, K. Mølmer, and E. S. Polzik, *Phys. Rev. Lett.* **79**, 4782 (1997).
- [25] E. G. Dalla Torre, J. Otterbach, E. Demler, V. Vuletić, and M. D. Lukin, *Phys. Rev. Lett.* **110**, 120402 (2013).
- [26] M. Tavis and F. W. Cummings, *Phys. Rev.* **170**, 379 (1968).
- [27] S. D. Bennett, N. Y. Yao, J. Otterbach, P. Zoller, P. Rabl, and M. D. Lukin, *Phys. Rev. Lett.* **110**, 156402 (2013).
- [28] H. Lipkin, N. Meshkov, and A. Glick, *Nuclear Physics* **62**, 188 (1965).
- [29] R. G. Unanyan and M. Fleischhauer, *Phys. Rev. Lett.* **90**, 133601 (2003).
- [30] L. D'Alessio, Y. Kafri, A. Polkovnikov, and M. Rigol, *Advances in Physics* **65**, 239 (2016).
- [31] T. Langen, T. Gasenzer, and J. Schmiedmayer, *Journal of Statistical Mechanics: Theory and Experiment* **2016**, 064009 (2016).
- [32] D. J. Wineland, J. J. Bollinger, W. M. Itano, F. Moore, and D. Heinzen, *Physical Review A* **46**, R6797 (1992).
- [33] R. H. Dicke, *Phys. Rev.* **93**, 99 (1954).
- [34] B. A. Chase and J. M. Geremia, *Phys. Rev. A* **78**, 052101 (2008).
- [35] R. J. Lewis-Swan, M. A. Norcia, J. R. K. Cline, J. K. Thompson, and A. M. Rey, *Phys. Rev. Lett.* **121**, 070403 (2018).
- [36] C. Gerry and P. Knight, *Introductory Quantum Optics* (Cambridge University Press, Cambridge, 2005).
- [37] K. Mølmer and A. Sørensen, *Phys. Rev. Lett.* **82**, 1835 (1999).
- [38] D. Leibfried, M. D. Barrett, T. Schaetz, J. Britton, J. Chiaverini, W. M. Itano, J. D. Jost, C. Langer, and D. J. Wineland, *Science* **304**, 1476 (2004).
- [39] D. Leibfried, E. Knill, S. Seidelin, J. Britton, R. B. Blakestad, J. Chiaverini, D. B. Hume, W. M. Itano, J. D. Jost, C. Langer, R. Ozeri, R. Reichle, and D. J. Wineland, *Nature* **438**, 639 (2005).
- [40] T. Holstein and H. Primakoff, *Phys. Rev.* **58**, 1098 (1940).
- [41] A. Kronwald, F. Marquardt, and A. A. Clerk, *New Journal of Physics* **16**, 063058 (2014).
- [42] R. G. Unanyan, *Theoretical and Mathematical Physics* **195**, 718 (2018).
- [43] R. G. Unanyan, C. Ionescu, and M. Fleischhauer, *Phys. Rev. A* **72**, 022326 (2005).
- [44] J. McKeever, J. R. Buck, A. D. Boozer, and H. J. Kimble, *Phys. Rev. Lett.* **93**, 143601 (2004).
- [45] I. Teper, Y.-J. Lin, and V. Vuletić, *Phys. Rev. Lett.* **97**, 023002 (2006).
- [46] K. M. Fortier, S. Y. Kim, M. J. Gibbons, P. Ahmadi, and M. S. Chapman, *Phys. Rev. Lett.* **98**, 233601 (2007).
- [47] N. Brahms, T. P. Purdy, D. W. C. Brooks, T. Botter, and D. M. Stamper-Kurn, *Nature Physics* **7**, 604 (2011).
- [48] H. Zhang, R. McConnell, S. Čuk, Q. Lin, M. H. Schleier-Smith, I. D. Leroux, and V. Vuletić, *Phys. Rev. Lett.* **109**, 133603 (2012).
- [49] Z. Chen, J. G. Bohnet, J. M. Weiner, K. C. Cox, and J. K. Thompson, *Phys. Rev. A* **89**, 043837 (2014).
- [50] J. Zeiher, J. Wolf, J. A. Isaacs, J. Kohler, and D. M. Stamper-Kurn, *arXiv preprint* (2020), 2012.01280.
- [51] J. Appel, P. J. Windpassinger, D. Oblak, U. B. Hoff, N. Kjærgaard, and E. S. Polzik, *Proceedings of the National Academy of Sciences* **106**, 10960 (2009).
- [52] T. Takano, M. Fuyama, R. Namiki, and Y. Takahashi, *Phys. Rev. Lett.* **102**, 033601 (2009).
- [53] M. H. Schleier-Smith, I. D. Leroux, and V. Vuletić, *Phys. Rev. Lett.* **104**, 073604 (2010).
- [54] J. G. Bohnet, B. C. Sawyer, J. W. Britton, M. L. Wall, A. M. Rey, M. Foss-Feig, and J. J. Bollinger, *Science* **352**, 1297 (2016).
- [55] J.-B. Béguin, J. H. Müller, J. Appel, and E. S. Polzik, *Phys. Rev. X* **8**, 031010 (2018).
- [56] V. Guarrera, R. Gartman, G. Bevilacqua, and W. Chalupczak, *arXiv preprint* (2020), 2012.12617v1.
- [57] A. C. Y. Li, F. Petruccione, and J. Koch, *Scientific Reports* **4**, 4887 (2014).
- [58] H. Häffner, C. F. Roos, and R. Blatt, *Physics Reports* **469**, 155 (2008).
- [59] J. Zhang, G. Pagano, P. W. Hess, A. Kyprianidis, P. Becker, H. Kaplan, A. V. Gorshkov, Z. X. Gong, and C. Monroe, *Nature* **551**, 601 (2017).
- [60] D. Porras and J. I. Cirac, *Physical Review Letters* **92**, 207901 (2004).
- [61] M. Eichenfield, J. Chan, R. M. Camacho, K. J. Vahala, and O. Painter, *Nature* **462**, 78 (2009).
- [62] M. J. Burek, J. D. Cohen, S. M. Meenehan, N. El-Sawah, C. Chia, T. Ruelle, S. Meesala, J. Rochman, H. A. Atikian, M. Markham, D. J. Twitchen, M. D.

- Lukin, O. Painter, and M. Lončar, *Optica* **3**, 1404 (2016).
- [63] J. V. Cady, O. Michel, K. W. Lee, R. N. Patel, C. J. Sarabalis, A. H. Safavi-Naeini, and A. C. Bleszynski Jayich, *Quantum Science and Technology* **4**, 024009 (2019).
- [64] D. A. Golter, T. Oo, M. Amezcua, K. A. Stewart, and H. Wang, *Physical Review Letters* **116**, 143602 (2016).
- [65] A. Albrecht, A. Retzker, F. Jelezko, and M. Plenio, *New Journal of Physics* **15**, 083014 (2013).
- [66] P. Macha, G. Oelsner, J.-M. Reiner, M. Marthaler, S. André, G. Schön, U. Hübner, H.-G. Meyer, E. Il'ichev, and A. V. Ustinov, *Nature Communications* **5**, 1 (2014).
- [67] K. V. Shulga, P. Yang, G. P. Fedorov, M. V. Fistul, M. Weides, and A. V. Ustinov, *JETP Letters* **105**, 47 (2017).
- [68] C. Song, K. Xu, H. Li, Y.-R. Zhang, X. Zhang, W. Liu, Q. Guo, Z. Wang, W. Ren, J. Hao, H. Feng, H. Fan, D. Zheng, D.-W. Wang, H. Wang, and S.-Y. Zhu, *Science* **365**, 574 (2019).
- [69] J. D. Brehm, A. N. Poddubny, A. Stehli, T. Wolz, H. Rotzinger, and A. V. Ustinov, *npj Quantum Materials* **6**, 10 (2021).
- [70] A. Bienfait, P. Campagne-Ibarcq, A. H. Küllerich, X. Zhou, S. Probst, J. J. Pla, T. Schenkel, D. Vion, D. Esteve, J. J. L. Morton, K. Mølmer, and P. Bertet, *Phys. Rev. X* **7**, 041011 (2017).
- [71] B. Albanese, S. Probst, V. Ranjan, C. W. Zollitsch, M. Pechal, A. Wallraff, J. J. L. Morton, D. Vion, D. Esteve, E. Flurin, and P. Bertet, *Nature Physics* **16**, 751 (2020).
- [72] M. A. Castellanos-Beltran, K. D. Irwin, G. C. H. van L R Vale, and K. W. Lehnert, *Nature Physics* **4**, 929 (2008).
- [73] X. Zhou, V. Schmitt, P. Bertet, D. Vion, W. Wustmann, V. Shumeiko, and D. Esteve, *Phys. Rev. B* **89**, 214517 (2014).
- [74] C. Macklin, K. O'Brien, D. Hover, M. E. Schwartz, V. Bolkhovskiy, X. Zhang, W. D. Oliver, and I. Siddiqi, *Science* **350**, 307 (2015).
- [75] N. Bergeal, F. Schackert, M. Metcalfe, R. Vijay, V. E. Manucharyan, L. Frunzio, D. E. Prober, R. J. Schoelkopf, S. M. Girvin, and M. H. Devoret, *Nature* **465**, 64 (2010).
- [76] D. Marković, S. Jezouin, Q. Ficheux, S. Fedortchenko, S. Felicetti, T. Coudreau, P. Milman, Z. Leghtas, and B. Huard, *Phys. Rev. Lett.* **121**, 040505 (2018).
- [77] M. Foss-Feig, Z.-X. Gong, A. V. Gorshkov, and C. W. Clark, *arXiv preprint* (2016), 1612.07805.
- [78] M. A. Perlin, C. Qu, and A. M. Rey, *Phys. Rev. Lett.* **125**, 223401 (2020).
- [79] C. W. Gardiner and P. Zoller, *Quantum Noise* (Springer-Verlag, Berlin Heidelberg, 2000).
- [80] G. S. Agarwal, R. R. Puri, and R. P. Singh, *Phys. Rev. A* **56**, 2249 (1997).
- [81] R. Kubo, *Journal of the Physical Society of Japan* **17**, 1100 (1962).
- [82] M. Zens, D. O. Krimer, and S. Rotter, *Phys. Rev. A* **100**, 013856 (2019).
- [83] S. G. Schirmer and X. Wang, *Phys. Rev. A* **81**, 062306 (2010).
- [84] R. Grimm, M. Weidemüller, and Y. B. Ovchinnikov, *Advances in Atomic, Molecular and Optical Physics Advances In Atomic, Molecular, and Optical Physics*, **42**, 95 (2000).
- [85] D. M. Brink and G. R. Satchler, *Angular momentum* (Clarendon Press, Oxford, 1968).
- [86] F. Damanet, D. Braun, and J. Martin, *Phys. Rev. A* **94**, 033838 (2016).
- [87] N. Shammah, S. Ahmed, N. Lambert, S. De Liberato, and F. Nori, *Physical Review A* **98**, 063815 (2018).
- [88] D. Bacon, I. L. Chuang, and A. W. Harrow, *Phys. Rev. Lett.* **97**, 170502 (2006).
- [89] P. A. Vetter, L. Wang, D.-W. Wang, and M. O. Scully, *Physica Scripta* **91**, 023007 (2016).